UNIVERSITY OF CALIFORNIA SAN DIEGO

Early Acquisition of $CD8^+$ T Cell Exhaustion State Is Regulated by Ezh2

A Dissertation submitted in partial satisfaction of the requirements
for the degree Doctor of Philosophy

in

Biomedical Sciences

by

Lauren Kainani Quezada

Committee in charge:

Professor John T. Chang, Chair
Professor Ananda Goldrath
Professor Stephen Hedrick
Professor Li-Fan Lu
Professor Elina Zuñiga

2022

The Dissertation of Lauren Kainani Quezada is approved, and it is acceptable in quality and form for publication on microfilm and electronically.

University of California San Diego

2022

DEDICATION

To my love, my father, my mother, and all of my families - through blood, through culture, through science, and those that are chosen

EPIGRAPH

Believe in yourselves. Dream. Try. Do good. I love you all. Class dismissed.

~ Mr. Feeny

TABLE OF CONTENTS

LIST OF ABBREVIATIONS

CFSE	Carboxyfluorescein succinimidyl ester
CUT&RUN	Cleavage under targets and release using nuclease
$Div1_{ARM}$	$CD8^+$ T cells responding to LCMV-Arm infection at division 1
$Div1_{CL13}$	$CD8^+$ T cells responding to LCMV-Cl13 infection at division 1
EV	Empty vector
FACS	Fluorescence activated cell sorting
GO	Gene Ontology
ISG	Interferon stimulated gene
LCMV-Arm	Lymphocytic choriomeningitis-Armstrong
LCMV-Cl13	Lymphocytic choriomeningitis-Clone 13
PCA	Principal Component Analysis
scRNA-seq	Single cell RNA-sequencing
scATAC-seq	Single cell Assay for Transposase-Accessible Chromatin-sequencing
S.E.M.	Standard error of the mean
T_{EX}	Exhausted $CD8^+$ T cells
UMAP	Uniform Manifold Approximation and Projection

LIST OF FIGURES

ACKNOWLEDGEMENTS

First, I would like to acknowledge and give my humblest thanks to my mentor, Dr. John T. Chang. One of my first exposures to UCSD and the Biomedical Sciences program, he was one of my interviewers as well as my first rotation mentor. He has provided me with unparalleled guidance and patience, especially through these past few years of the pandemic. Through his leadership, I slowly overcame unanticipated hurdles and made it to the finish line. He has further instilled in me the values of perseverance, dedication and reinforced my passion for science. He has always held my best interests at heart and allowed me time to grow and learn. I will forever be grateful to him and the lab whose people and culture he has carefully cultivated.

All of these people, my lab family, also need to be acknowledged. Stella Widjaja as my first graduate student mentor through my rotation and my first year in the lab. She laid the foundation of molecular and *in vivo* mouse work – two areas I knew almost nothing about. She paved the way for the beginnings of my thesis work, exposing me to transcriptomics and method development. I would not be where I am without her helping hand. Thank you to the lab managers and mouse colony wizards present during my time in the lab, Justine Lopez, Tiffani Tysl & Cynthia Indralingam who kept me on track with mice and ensuring I knew exactly what I had to work with. They were constantly in the background making sure that all of our basics were stocked and ready for use. Jocelyn Olvera, Nadia Kurd & Shefali Patel, you all kept my mind at ease whether in a scientific capacity or moral support. I know I will always be able to count on you for advice, silliness and a lifetime of memories. The Dream Team, my forever undergrads, who are now fulfilling their destinies in medical school. I need to thank these three,

Eleanor Kim, Han Duong, and Abigail Limary, for assisting me in every way possible - the late nights running to IGM or going on boba runs I will never forget. Paul Hsu, Matthew Tsai, Brigid Boland, Jane Klann & Daniel Garcia, I considered them all “lab elders” with endless amounts of knowledge and ideas. All of them are scientists and people I aspire to. Emily Liu, Priscilla Yao & Elena Lin came into my life towards the end of my time in the lab. Emily, my best student and the best underling I could ask for. Priscilla and Elena, you both brought humor, doodles, baked goods and scientific input that I value so. Last, but not least, Tiani Louis. She has been a light in the darkness, a shoulder to cry on and the first I would want to celebrate anything with. A brilliant woman and talented scientist, she taught me the value of balancing time and life and acknowledging that sometimes we all need a push and a little help sometimes. She kept me afloat more than she can know.

My wonderful committee, Ananda Goldrath, Elina Zúñiga, Li Fan Lu & Steve Hedrick, made sure that I kept on track in my understanding of the direction of my project in the kindest and most constructive way. My appreciation for the nuance of a scientific narrative only increased with your input and guidance. Further, I need to acknowledge Zharoen He and Wenhao Jin of the Yeo lab for your precious time in conducting all of the computational work in this thesis. This project would have gone nowhere without you – your expertise in these matters shines through in all I have seen you do. Thank you both for keeping my datasets in your careful hands.

Thank you to Dr. Martina Ramirez, for being my first mentor in undergrad. She taught me the potential of scientific research through allowing me to be a “spider-ling” and showing me the entry door in the form of field work and ecology. Dr. Christina King-

Smith taught me scientific endurance in gaining my Master's degree, pushing me through the many obstacles encountered in that time.

Perhaps most importantly, I need to thank my family. My love and soon to be husband, Ryan Urak, our friendship and romance was kindled at City of Hope in the Forman lab working in immunotherapeutics – planting the seed for love of immunology and a love for you. Your passion for science was and is infectious and has never left me. As difficult as it was to be apart for all of these years, I knew you were always there to catch me if I fell, keep my head in the game, and scientific perspective open. To my mom and dad, Christine Aiu-Quezada and Jorge Quezada, you encouraged my love of learning from the beginning and supported me through any difficulties I had growing up. You never let me falter and afforded me all of the opportunities I never knew existed or needed to ask for. Thank you for your unwavering love. To all members of all of my families which this entire degree is dedicated to, my family through blood, through friendship, through BMS, and through my beloved hālau, I could not have done this without you.

Chapters 1, 2, and 3 in full, are an adapted version of the material that has been submitted for publication. Lauren K. Quezada, Wenhao Jin, Yi Chia Liu, Eleanor S. Kim, Zhaoren He, Cynthia S. Indralingam, Tiffani Tysl, Lara Labarta-Bajo, Ellen J. Wehrens, Yeara Jo, Katelynn Kazane, C.J. Hattori, Elina I. Zuniga, Gene W. Yeo, John T. Chang (2022). Early acquisition of phenotypic, transcriptional, and epigenetic features associated with T cell exhaustion. In revision. The dissertation author was primary author of all material.

VITA

2008 B.S., Biology, Loyola Marymount University

2013 M.A., Biological Sciences, Saint Joseph's University

2022 Ph.D., Biomedical Sciences, University of California San Diego

ABSTRACT OF THE DISSERTATION

Early Acquisition of $CD8^+$ T Cell Exhaustion State Facilitated by Ezh2

by

Lauren Kainani Quezada

Doctor of Philosophy in Biomedical Sciences

University of California San Diego, 2022

Professor John T. Chang, Chair

During infection with an acute microbial infection, responding $CD8^+$ T cells give rise to effector cells that provide acute host defense and memory cells that provide sustained protection. An alternative outcome is exhaustion, a state of T cell dysfunction that occurs in the context of chronic infections and cancer. Although it is evident that exhausted $CD8^+$ T cells (T_{EX}) are phenotypically and molecularly distinct from effector and memory $CD8^+$ T cells, the factors regulating the earliest events in the differentiation process of T_{EX} cells remain incompletely understood. Here we performed single-cell RNA-sequencing and single-cell ATAC-sequencing of $CD8^+$ T cells responding to LCMV-Armstrong (LCMV-Arm) or LCMV-Clone 13 (LCMV-Cl13). Compared to $CD8^+$ T cells that had undergone their first division in response to LCMV-Arm ($Div1_{ARM}$) cells, $CD8^+$ T cells that had undergone their first division in response to LCMV-Cl13 ($Div1_{CL13}$) expressed higher levels of genes encoding transcription factors that have been previously reported to promote exhaustion, along with Ezh2, the catalytic component of the polycomb repressive complex 2 (PRC2) complex which mediates epigenetic silencing. Modulation of Ezh2 by genetic deletion or retroviral overexpression approaches resulted in decreased or increased expression, respectively, of exhaustion-associated molecules by $CD8^+$ T cells responding to LCMV-Cl13. Taken together, these findings indicate that acquisition of phenotypic, transcriptional, and epigenetic features associated with T cell exhaustion can occur earlier than previously appreciated and raise the possibility that T_{EX} cells may not need to transit through an effector intermediate state.

INTRODUCTION

$CD8^+$ T Cell Response to Acute and Chronic Infection

Acute microbial infection results in a well documented immune response. Firstly, antigen-specific naïve $CD8^+$ T cells will recognize their cognate antigen by MHC (major histocompatibility complex) binding with antigen presenting cells (APCs). These T cells will then undergo activation, partially mediated by pro-inflammatory cytokines such as IL-12, IL-2 and Type I interferons (IFN-1) to augment their expansion. Upon differentiation, effector T cells provide acute host defense and memory cells that provide sustained protection (Chang, Wherry and Goldrath 2014). Cytotoxic effector T cells secrete inflammatory cytokines such as IFNγ and TNF, along with cytolytic granules, such as granzymes and perforin, to kill infected cells. Many of these effector T cells will die via apoptosis following viral clearance and memory T cells will further differentiate into T_{CM} (central memory T cells), T_{EM} (effector memory T cells), which remain in ciruclation, or T_{RM} (resident memory T cells), which home to specific tissue, and overtake the population. These are antigen independent, long-lived cells whose proliferation is homeostatically maintained and survive through the reception of interleukin-7 and interleukin-15. These memory T cells are distinguished from effector cells largely by the expression of KLRG1 (killer cell lectin-like receptor subfamily G member 1) and IL-7R (interleukin-7 receptor, CD127) and serve to provide a rapid response upon reinfection. However, an alternative outcome to the generation of effector and memory cells is exhaustion, which occurs in the setting of chronic infections and tumors, resulting in T cells that exhibit a reduced functional capacity (Wherry 2011, Wherry and Kurachi 2015, Angelosanto et al. 2012).

Lymphocytic choriomeningitis virus (LCMV) is a noncytopathic RNA arenavirus allowing for a direct study of the host response to infection apart from direct cellular damage of the virus and is a well-characterized model system that has been extensively used to study $CD8^+$ T cell responses to acute and chronic infections. Acute infection with the LCMV-Armstrong (LCMV-Arm) strain results in clearance of the infection in 7-10 days and the generation of effector and memory T cells. By contrast, chronic infection with the LCMV-Clone 13 (LCMV-Cl13) strain results in persistent antigen and T cell exhaustion. LCMV-Cl13 differs from LCMV-Arm by two amino acids, conferring a persistent infection, remaining in circulation from 60-90 days (Bocharov, Argilaguet and Meyerhans 2015, MS 2019). Generally, in this time exhausted $CD8^+$ T (T_{EX}) cells exhibit an increased expression of inhibitory receptors such as PD1, LAG3, TIM3, CTLA4, and TIGIT; reduced proliferative capacity when stimulated; and a hierarchical loss of cytokine production and function. The severity of this exhausted phenotype depends on the severity of the initial infection and time of persistence (Wherry 2011, Wherry and Kurachi 2015, Muroyama and Wherry 2021). In the most severe cases, T cell exhaustion can lead to deletion of T cells and thus result in failure to efficiently clear the microbial pathogen. The exhaustion phenotype is also seen in a reduced capacity to generate a healthy pool of heterogenous memory T cells. It is important to note that T_{EX} cells are hypofunctional and not rendered completely inactive.

Compared to effector and memory T cells, T_{EX} cells exhibit an altered transcriptional program involving multiple transcription factors, including TOX, NFAT, IRF4, BATF, and NR4A family members, as well as a unique epigenetic landscape (McLane, Abdel-Hakeem and Wherry 2019, Martinez et al. 2015, Yao et al. 2019, Khan

et al. 2019, Alfei et al. 2019, Seo et al. 2019, Scott et al. 2019, Chen et al. 2019a, K et al. 2017). Furthermore, recent studies have identified heterogeneity within the T_{EX} cell population. For example, T_{EX} cells have been subdivided into three states, a progenitor or precursor state characterized by high expression of TCF1, SLAMF6, and CXCR5, along with low levels of T-bet; an intermediate or transitory state characterized by high levels of T-bet, CX3CR1, TIM3, and low levels of Eomes; and a terminal state characterized by high expression of TIM3, CD101, and Eomes, along with low levels of T-bet (Paley et al. 2012, DT et al. 2016, Im et al. 2016, Beltra et al. 2020, Chen et al. 2019b, Wang et al. 2019, Hudson et al. 2019).

Overall, chronic infection alters behavior of multiple immune cell subsets as well as various signaling and metabolic pathways. The change of the immune response to chronic versus acute infection affects $CD8^+$ T cell response from antigen presentation to final effector function. Previously, our lab investigated the response of $CD8^+$ T cells to LCMV-Arm using single-cell RNA sequencing (scRNA-seq) and revealed two separate clusters at division 1 post-infection, showing a novel, very early fate divergence. These cells separated into two distinct clusters whose transcriptional profiles closely resembled either that of terminal effector T cells or of memory T cells (Kakaradov et al. 2017). This dissertation, in part, further investigates early heterogeneity by similarly using scRNA-seq to identify distinctions of transcriptional landscapes between $CD8^+$ T cells responding to acute versus chronic infection at division 1.

The Role of Ezh2 in $CD8^+$ T Cell Differentiation and Immune Cell Exhaustion

Polycomb Group proteins (PcG) function as gene repressors and are highly active during embryonic development, cellular differentiation and memory formation.

Polycomb repressive complex (PRC) 1 and PRC2 are members of this family responsible for epigenetic control by ubiquitination or methylation respectively. Focusing on PRC2, it is evolutionarily conserved and consists of 4 subunits; Rbbp4 (RB binding protein 4) and a trimeric core of Suz12, Eed and Ezh1 or Ezh2 (Enhancer of zeste homologue 1 or 2). In line with the larger PcG protein family, the main function of PRC2 is gene suppression by the tri-methylation of histone H3 lysine 27, a mark of chromatin silencing. Ezh1 and Ezh2 are catalytic components of this complex containing a SET domain responsible for its methyltransferase activity. Only one of these is present in a given PRC2 complex. Ezh1 is found in either differentiated or dividing cells, while Ezh2 is only detected in actively dividing cells. Ezh1 as a component of PRC2 greatly decreases its methyltransferase activity compared to Ezh2. Previous studies suggest that Ezh2 is majorly responsible for the primary deposition of suppressive tri-methyl marks to histone 3 while Ezh1 restores it. If these marks were lost due to demethylases or other biological processes, Ezh1 will be most efficient at replacing them (Margueron and Reinberg 2011, Aranda, Mas and Croce 2015, Chammas, Mocavini and Di Croce 2019).

The role of Ezh2 in Th1 and Th2 helper $CD4^+$ cells and regulatory T cell development has been extensively studied. Ezh2 facilitates helper T cell lineage definition by binding, and thus silencing through H3K27 tri-methylation, to *Tbx21* or *Gata3*. As *Tbx21* induces Th1 development while *Gata3* induces Th2, repressing either of these genes regulate helper T cell lineage progression. (Tumes et al. 2013, DuPage et al. 2015, Yang et al. 2015, Chen et al. 2020). In $CD8^+$ T cells, Ezh2 is known to have an important role not only in their differentiation in response to acute infection but also in

T cell development. Even before T cells are generated, Ezh2 maintains the stemness of hematopoietic stem cells repressing such genes as *Cdkn2*. Once in the thymus, studies have found that regulation of thymocyte development is dependent on Ezh2-mediated silencing of cell cycle inhibitors. (Cordero et al. 2017, Huang et al. 2021a, Wang et al. 2018). However, maturation of T cells is not affected by the loss of either Ezh1 or Ezh2 function but this loss does slightly reduce their numbers in lymphoid tissue (Dobenecker et al. 2018). When MHC molecules on naïve $CD8^+$ T cells bind their cognate antigen to the adaptive immune response is initiated. Upon acute infection by LCMV-Arm, previous studies have shown *Ezh2* is quickly upregulated, as early as the first division, in precursor terminal effector cells as compared to a precursor memory population. (Kakaradov et al. 2017). In the context of cancer, aberrant expression of the PRC2 complex plays a role in either promoting tumor growth by PRC2 loss or gain of function mutations or preventing tumor onset by promoting repair of dsDNA (double stranded DNA) breaks (Laugesen, Højfeldt and Helin 2016). However, the role of Ezh2 in the regulation of $CD8^+$ T cell exhaustion via chronic infection is not fully understood.

In this dissertation, we use a used scRNA-seq and scATAC-seq (assay for transposase-accessible chromatin with high-throughput sequencing) to observe differences in the transcriptomic and epigenetic landscapes of $CD8^+$ T cells responding to acute versus chronic infection as early as division 1. scRNA-seq reveals LCMV-Arm infection resulting in two distinct populations, as expected, and LCMV-Cl13 infection clustering separately and as a single population; a previously unseen phenomenon. Further, differential gene expression analysis shows an upregulation of multiple inhibitory receptors and transcription factors typically associated with T cell exhaustion

as well as genes involved in epigenetic regulation and interferon stimulated genes. scATAC-seq analysis similarly reveals a separate clustering of areas of chromatin accessibility between acute and chronic infection. We further investigated the impact of *Ezh2* expression and its potential mediation by *Ifnar1* as both genes are known to have a major role in epigenetic regulation. We found that the ablation or reduction of *Ezh2* expression yields rescue of T cell exhaustion, while forced expression of *Ezh2* results in an exacerbation of this phenomenon. Our study also demonstrates that the expression and function of IFNAR1 may mediate Ezh2 expression as early as division 1 thus regulate $CD8^+$ T cell exhaustion via epigenetic silencing. Together, these findings reveal the possibility that exhausted T cell fate may diverge from that of canonical effector or memory T cells earlier than previously thought; perhaps differentiating into a pre-cursor exhausted state much earlier than previously thought, without passing through progenitor and intermediate exhausted stages.

CHAPTER 1: CHRONIC INFECTION YIELDS AN EARLY DIVERGENCE OF EXHAUSTED CD8$^+$ T CELL FATE

1.1: Introduction

To date, the effect of persistent antigen has on various immune cell subsets has been studied in various infection and cancer models. LCMV-Cl13 infection results in hypofunctionality in natural killer cells, myeloid dendritic cells, CD4$^+$ helper T cells and most extensively studied, CD8$^+$ T cells. The timing and precise sequence of events regulating CD8$^+$ T cell exhaustion remain incompletely understood. In particular, do T_{EX} cells transit from a functional effector state prior to commencing the exhaustion program, or can they bypass a functional intermediate effector state soon after activation? Previous studies have shown a divergence of CD8$^+$ T cells responding to acute vs. chronic infection at day 4.5 at the earliest by scRNA-seq (Khan et al. 2019). In this chapter, we again performed scRNA-seq comparing LCMV-Arm to LCMV-Cl13 and extended the experimental time course from day 2 to day 60 post-infection. We found a striking difference in the transcriptional patterns between the viral conditions as early as division 1. Among these we see an upregulation of inhibitory receptors, exhaustion associated genes, and interferon stimulated genes in CD8$^+$ T cells responding to LCMV-Cl13 compared to LCMV-Arm. We further confirmed this distinction at the epigenetic level with scATAC-seq analysis. We conclude that there is a clear divergence in transcriptional patterns, expression dynamics, and epigenetics of CD8$^+$ T cells responding to acute vs. chronic infection as early as division 1.

1.2: Results

1.2.1: scRNA-seq reveals transcriptional heterogeneity in CD8$^+$ T cell response to acute vs. chronic infection

Previous studies from our lab have shown early heterogeneity via scRNA-seq in acute infection. To expand these studies, we compared CD8$^+$ T cells responding to acute vs. chronic infection, CD8$^+$CD45.1$^+$ P14 T cells, which have transgenic expression of a T cell receptor (TCR) that recognizes an immunodominant epitope of LCMV. We adoptively transferred these into congenic CD45.2 recipients subsequently infected with LCMV-Arm or LCMV-Cl13. For some experiments, in order to identify cells that had undergone their first division, CD8$^+$ P14 T cells were first labeled with the proliferation dye carboxyfluorescein succinimidyl ester (CFSE) prior to transfer. Recipient mice were sacrificed at 9 time points: days 2 (Division 1, 'Div1'), 4, 5, 6, 7, 8, 22, 34, and 60 post-infection. Naïve CD8$^+$ P14 T cells (CD62L^{hi}CD44^{lo}) were also included as a control. Donor CD8$^+$CD45.1$^+$ P14 T cells were FACS-purified at each time point and processed for scRNA-seq with the 10x Genomics Chromium platform (**Figure 1.1A**).

To investigate the transcriptional differences between CD8$^+$ T cells responding to acute vs. chronic infection, we analyzed the data from all time points together and performed Uniform Manifold Approximation and Projection (UMAP) analyses. CD8$^+$ T cells separated into 17 clusters (**Figure 1.1B, left**) on the basis of infection type (LCMV-Arm vs. LCMV-Cl13) (**Figure 1.1B, middle**) and time points (**Figure 1.1B, right**). CD8$^+$ T cells that had undergone their first division (2nd CFSE peak, **Figure 1.2A**) in response to LCMV-Arm infection separated into two clusters (**Figure 1.1B, right**), as previously

observed (Kakaradov et al. 2017). Strikingly, $CD8^+$ T cells that had undergone their first division in response to LCMV-Cl13 infection formed a single cluster that was distinct from the two LCMV-Arm Div1 clusters (**Figure 1.1B, right**) indicating a loss of heterogeneity with chronic infection.

Most clusters were made up of only cells responding to either LCMV-Arm or LCMV-Cl13 (**Fig 1.1C**). For example, Clusters 1, 3, 4, 6, 9, 10, and 12 were mostly comprised of cells responding to LCMV-Arm, whereas Clusters 7, 13 and 8 were primarily comprised of cells responding to LCMV-Cl13. The remainder of the clusters were comprised of mixtures of cells responding to either LCMV-Arm or LCMV-Cl13. Hierarchical clustering analyses grouped clusters exhibiting similar gene expression patterns (**Figure 1.1D**). Notably, grouping of clusters was driven by infection type, but also correlated with the time point after infection.

1.2.2: Transcriptional, epigenetic & phenotypic $CD8^+$ T cell response to acute vs. chronic infection diverges as early as division 1

Next, to investigate the distinct clustering of $CD8^+$ T cells that had undergone their first division in response to LCMV-Arm vs. LCMV-Cl13, we analyzed the gene expression patterns of the three Div1 clusters. One of the two LCMV-Arm Div1 clusters expressed molecules associated with memory $CD8^+$ T cells, whereas the other LCMV-Arm Div1 cluster expressed factors associated with terminal effector cell differentiation (**Figure 1.2B**). We therefore annotated these two LCMV-Arm clusters as '$Div1_{ARM\text{-}MEM}$' and '$Div1_{ARM\text{-}EFF}$' because phenotypically similar clusters were previously shown to exhibit disparate tendencies to give rise to memory and effector $CD8^+$ T cells

(Kakaradov et al. 2017); the single LCMV-Cl13 cluster was annotated as 'Div1$_{CL13}$.' Pathway analyses of genes differentially expressed by the three Div1 clusters revealed an enrichment of genes related to proliferation, transcriptional and epigenetic regulation, and chromatin modifying enzymes in the Div1$_{CL13}$ cluster (**Figure 1.2C**).

Focusing next on specific genes, we observed that transcription factors previously associated with memory CD8$^+$ T cells, such as *Lef1*, *Eomes*, *Tcf7*, and *Id3,* were more highly expressed by Div1$_{ARM-MEM}$ cells than by cells from either of the other two Div1 clusters. By contrast, transcription factors including *Batf*, *Irf4*, and *Nfatc1,* which have been previously reported to promote exhaustion (Chen et al. 2021, K et al. 2017, Martinez et al. 2015), were more highly expressed by Div1$_{Cl13}$ cells. Furthermore, *Ezh2* and *Suz12*, which encode components of the PRC2 complex that mediates epigenetic silencing (SM et al. 2017, Kakaradov et al. 2017) were more highly expressed by Div1$_{Cl13}$ cells. Lastly, Div1$_{Cl13}$ cells expressed high levels of genes that encode molecules previously associated with exhaustion, including *Havcr2* (Tim3), *Lag3*, and *Pdcd1*, along with genes controlling responsiveness to cytokines including IL-2 and type I interferons (IFN-I) (**Figure 1.2A**). Analyses of protein expression with flow cytometry experiments confirmed findings observed at the transcriptional level (**Figure 1.2D**).

1.2.3: Epigenetic and transcriptional dynamic heterogeneity is found in CD8$^+$ T cells responding to acute vs. chronic infection

To investigate whether the transcriptional heterogeneity observed in Div1 cells was accompanied by epigenetic heterogeneity, we performed scATAC-seq on Div1

cells. UMAP analyses using the scATAC-seq data revealed that Div1 cells separated into 4 clusters, three of which were derived from cells responding to LCMV-Cl13, and the other derived from cells responding to LCMV-Arm (**Figure 1.3A**). Intriguingly, additional analyses revealed that distinct sets of transcription factor binding motifs were preferentially enriched within differentially accessible chromatin peaks from the three Div1-Cl13 clusters. For example, BATF and AP-1 family transcription factors such as Fos and Jun were enriched in Div1-Cl13 Cluster 1; LEF and TCF transcription factors were enriched in Div1-Cl13 Cluster 3; and T-box transcription factors T-bet and Eomes were enriched in Div1-Cl13 Cluster 4 (**Figure 1.3B-D**). Taken together, these findings indicate that acquisition of phenotypic, transcriptional, and epigenetic characteristics associated with T cell exhaustion can occur earlier than previously appreciated, raising the possibility that $CD8^+$ T cells can enter a pre-exhausted precursor state soon after activation.

To gain further insight into this possibility, we applied scVelo, a previously published framework to analyze transcriptional dynamics of splicing kinetics using a likelihood-based dynamical model (La Manno et al. 2018, V et al. 2020). Application of scVelo to Div1 cells suggested that LCMV-Arm Div1 and LCMV-Cl13 Div1 cells did not share a common differentiation pathway (**Figure 1.4A**). Moreover, putative driver genes identified by scVelo as regulating differentiation in response to LCMV-Cl13, such as *Batf3*, were largely distinct from putative driver genes identified for differentiation in response to LCMV-Arm (**Figure 1.4B**), supporting the hypothesis that $CD8^+$ T cells responding to LCMV-Arm vs. LCMV-Cl13 may undertake distinct differentiation paths very early on.

1.3: Discussion

Recently, a study using a combination of scRNA-seq, lineage tracing, and genetic perturbations defined some of the early features of T_{EX} cell formation (Chen et al. 2019b). Specifically, TCF1 was shown to govern early events by antagonizing genes that promote terminal effector differentiation while positively regulating Eomes and c-Myb. Conversely, other studies have shown that the the transcription factor TOX facilitates the fate of terminally exhausted T cells. Increased expression of the inhibitory receptors and transcription factors associated with exhaustion as well as decreased secretion of inflammatory cytokines occur in response to TOX expression. Together these actions orchestrated a divergence of the T_{EX} cell vs. terminal effector cell differentiation pathways that was evident by day 8 following infection with LCMV-Cl13. Our observations extend these findings by showing that $CD8^+$ T cells that have undergone their first division in response to LCMV-Cl13 already exhibit phenotypic, transcriptional, and epigenetic features previously associated with T_{EX} cells. In particular, compared to $Div1_{ARM}$ cells, $Div1_{CL13}$ cells exhibited higher expression of transcription factors that have been implicated in promoting exhaustion, including NRF4A (Chen et al. 2019a), IRF4 (K et al. 2017), and NFAT (Martinez et al. 2015). Phenotypically, increased expression of exhaustion associated molecules is also observed at division 1 in chronic infection.

scVelo analysis also revealed a distinction in splicing kinetics between LCMV-Arm and LCMV-Cl13 infection specifying early putative exhaustion drivers such as *Batf3*. However, recent studies have shown that *Batf3* abrogates the exhaustion

phenotype in LCMV-Cl13 infection once chronicity has been reached. P14 cells transduced with either *Batf3* or empty vector were co-transferred into mice which had been infected with LCMV-Cl13 30 days prior. By day 7 post-transfer, there were a higher number of cells which overexpressed *Batf3* in comparison to the control as well as an increase IFNγ secretion indicating exhaustion rescue (Ataide et al. 2020). This discrepancy can potentially be explained due to the timing of increased *Batf3* expression or simply biological context. Similar to *Batf*, which can function as an enhancer of either effector function or exhaustion, *Batf3* may have the differential effects of facilitating exhaustion early while driving the memory $CD8^+$ T cell phenotype (Martinez et al. 2015, Quigley et al. 2010, Kurachi et al. 2014, Seo et al. 2021).

In addition, scATAC-seq results showed a distinct clustering of $CD8^+$ T cells responding to LCMV-Arm from those responding to LCMV-Cl13 at division 1 post-infection. This shows a divergence in areas of chromatin accessibility very early in chronic infection. Interestingly, $CD8^+$ T cells responding to LCMV-Cl13 does not show transcriptional heterogeneity at division 1 by scRNA-seq. Yet, epigenetic heterogeneity is seen in the LCMV-Cl13 cluster generated by scATAC-seq analysis. This cluster further separates into 3, showing each cluster to have a distinct set of enriched transcription factor motifs between them. Cluster 1 is enriched for BATF and AP-1 family members, typically associated with terminal exhaustion; and cluster 2 with TCF and LEF transcription factors, tightly associated with exhaustion “stem-ness”. T-box transcription factors, Tbet and EOMES are enriched in cluster 3. $Tbet^{hi}EOMES^{lo}PD1^{int}$ exhausted $CD8^+$ T cells are more prone to pharmocological rescue by anti-PD1 therapy in cancer and promote exhaustion “stem-ness”. Conversely, $Tbet^{lo}EOMES^{hi}PD1^{int}$ are

more fated to terminal exhaustion and deletion (Pauken and Wherry 2015, Paley et al. 2012).

Chapter 1, in full, is an adapted version of the material that has been submitted for publication. Lauren K. Quezada, Wenhao Jin, Yi Chia Liu, Eleanor S. Kim, Zhaoren He, Cynthia S. Indralingam, Tiffani Tysl, Lara Labarta-Bajo, Ellen J. Wehrens, Yeara Jo, Katelynn Kazane, C.J. Hattori, Elina I. Zuniga, Gene W. Yeo, John T. Chang (2022). Early acquisition of phenotypic, transcriptional, and epigenetic features associated with T cell exhaustion. In revision. The dissertation author was primary author of all material.

Figure 1.1 Single-cell RNA-sequencing analyses of $CD8^+$ T cells responding to acute vs. chronic infection. (A) Experimental setup. $CD45.1^+CD8^+$ P14 T cells were adoptively transferred into separate $CD45.2^+$ hosts 1 day prior to infection with either LCMV-Arm or LCMV-Cl13. To identify cells that had undergone their first division, some cells were labeled with CFSE prior to adoptive transfer. Splenocytes were harvested at the indicated time points after infection. Donor P14 $CD8^+$ T cells were FACS-isolated and processed for scRNA-seq using the 10x Chromium Genomics platform. **(B)** UMAP clustering of all $CD8^+$ cells, colored by cluster identity (left), infection type (middle), or time point (right). Number of cells transferred for each time point indicated to the right of the time point UMAP. **(C)** Bar graphs indicating the infection type and time point from which cells derived from each cluster are derived; clusters are grouped according to similarity in gene expression based on (D). **(D)** Hierarchical clustering of clusters based on gene expression profiles.

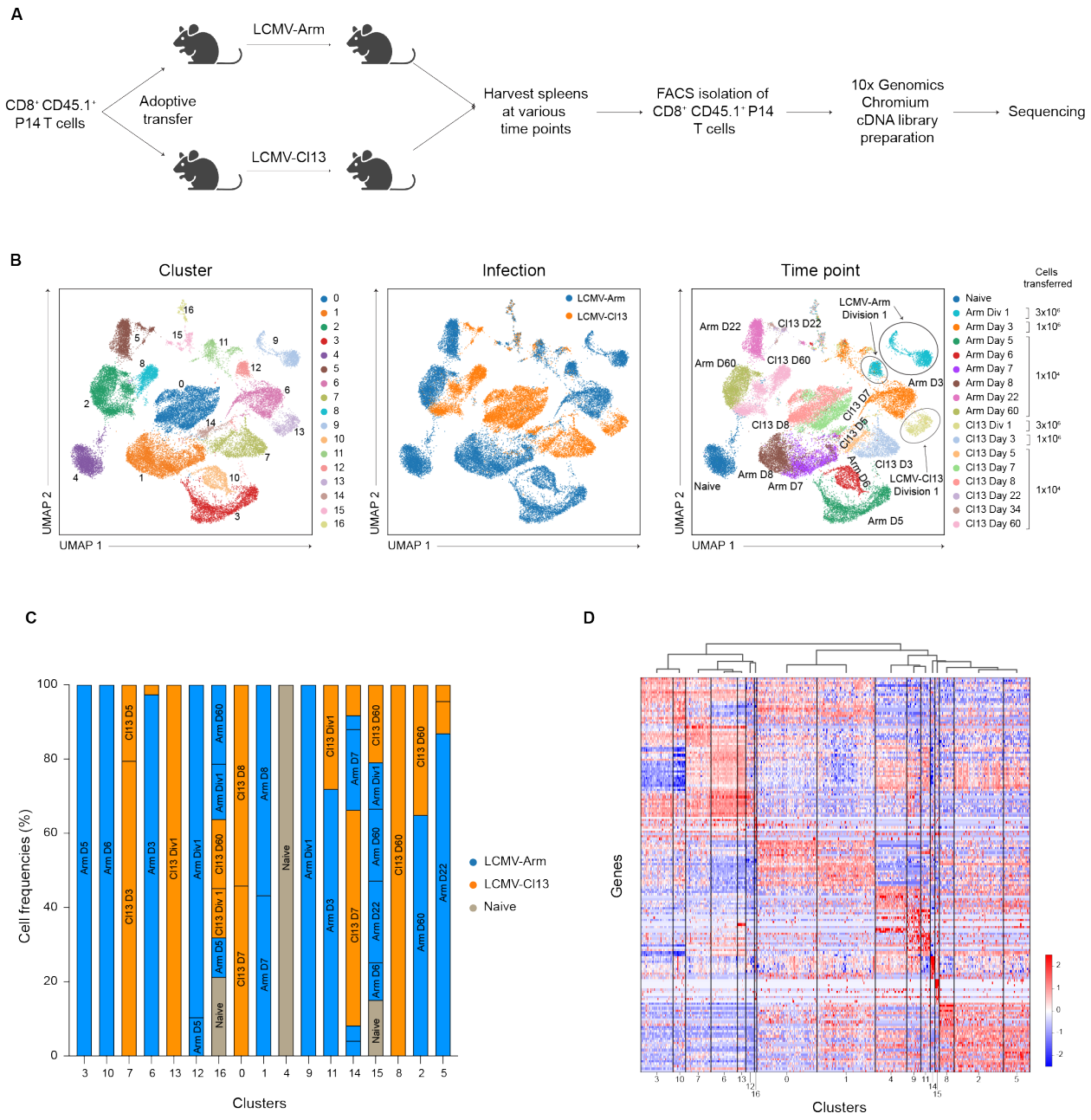
A
LCMV-Arm
CD8+ CD45.1+
P14 T cells
Adoptive
transfer
LCMV-Cl13
Harvest spleens
at various
time points
FACS isolation of
CD8+ CD45.1+ P14
T cells
10x Genomics
Chromium
cDNA library
preparation
Sequencing
B
Cluster
Infection
Time point
Cells
transferred
UMAP 1
UMAP 2
LCMV-Arm
LCMV-Cl13
Arm D22
Cl13 D22
LCMV-Arm
Division 1
Arm D60
Cl13 D60
Arm D3
Cl13 D7
Cl13 D8
Cl13 D5
Cl13 D3
Arm D8
Arm D7
Arm D6
Naive
LCMV-Cl13
Division 1
Arm D5
Naive
Arm Div 1
Arm Day 3
Arm Day 5
Arm Day 6
Arm Day 7
Arm Day 8
Arm Day 22
Arm Day 60
Cl13 Div 1
Cl13 Day 3
Cl13 Day 5
Cl13 Day 7
Cl13 Day 8
Cl13 Day 22
Cl13 Day 34
Cl13 Day 60
3x10^6
1x10^6
1x10^4
3x10^6
1x10^6
1x10^4
C
Cell frequencies (%)
Clusters
LCMV-Arm
LCMV-Cl13
Naive
D
Genes
Clusters

Figure 1.2 $CD8^+$ T cells that have undergone their first division in response to LCMV-Arm vs. LCMV-Cl13 exhibit phenotypic and transcriptional heterogeneity. **(A)** Gating strategy for CFSE stained $CD8^+CD45.1^+$ P14 T cells that had undergone their first division FACS purification (2^{nd} CFSE peak) and flow cytometry analysis. **(B)** Heatmaps representing relative gene expression of the three Division 1 clusters, $Div1_{ARM\text{-}EFF}$, $Div1_{ARM\text{-}MEM}$, and $Div1_{CL13}$, divided by category; rows represent selected genes and columns represent each of three Division 1 clusters. **(C)** Pathway analysis of $Div1_{ARM\text{-}EFF}$, $Div1_{ARM\text{-}MEM}$, and $Div1_{CL13}$. **(D)** Representative flow cytometry plots (left) displaying expression of Ezh2, CD25 (IL-2Rα), CD44, and T-bet protein among gated Division 1 (2^{nd} CFSE peak) P14 T cells. Bar graphs indicate the frequencies (middle) or mean fluorescence intensity (MFI, right) of P14 T cells responding to LCMV-Arm (blue) or LCMV-Cl13 (red) expressing each molecule. Data are shown as mean ± SEM. *p < 0.05, **p < 0.01, ***p < 0.0001, ****p < 0.0001 (paired t test). Data are representative of 2 to 3 independent experiments.

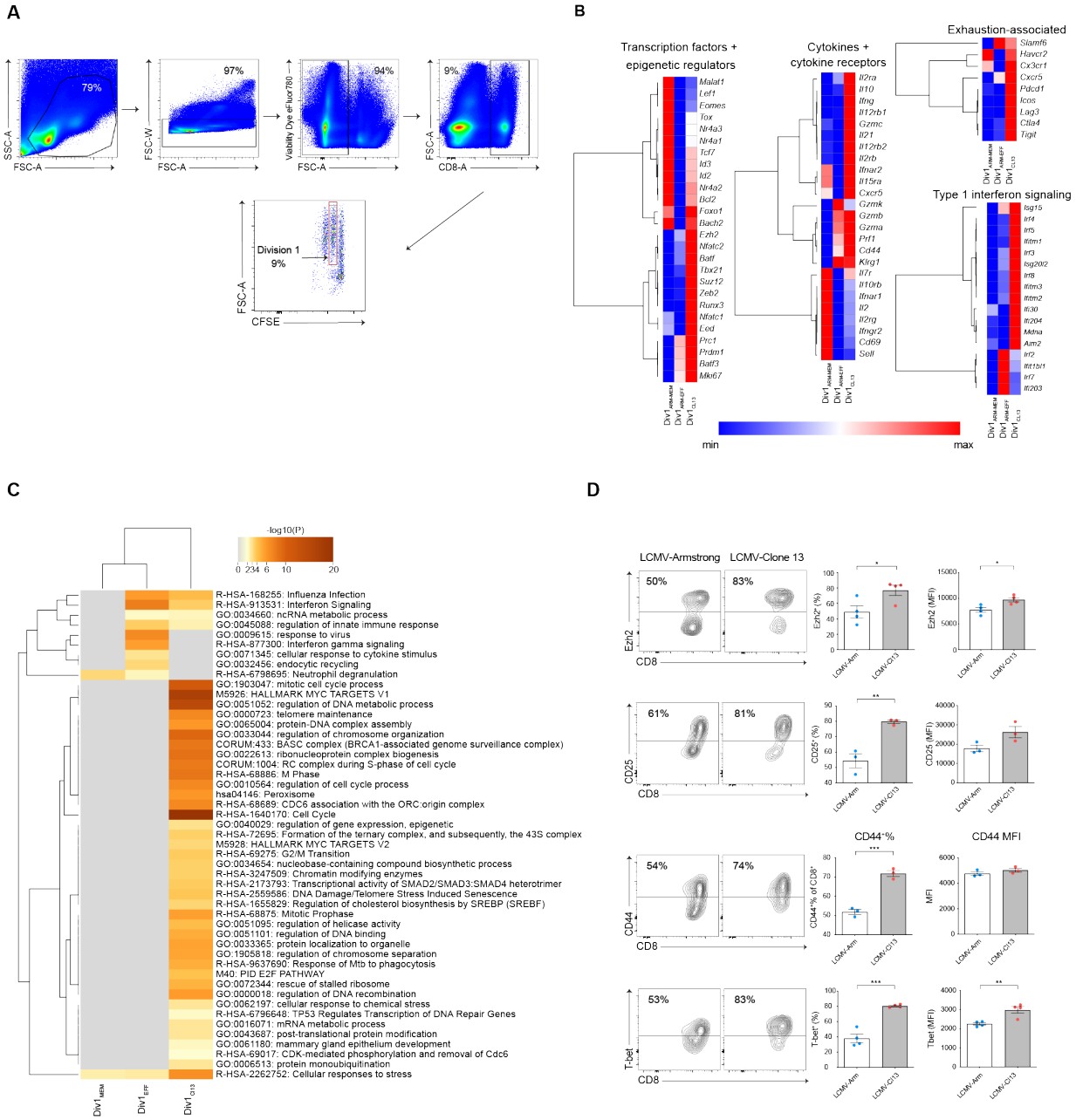
A
SSC-A
FSC-A
79%
FSC-W
97%
Viability Dye eFluor780
94%
FSC-A
CD8-A
9%
Division 1
9%
CFSE
B
Transcription factors +
epigenetic regulators
Cytokines +
cytokine receptors
Exhaustion-associated
Type 1 interferon signaling
min
max
C
-log10(P)
R-HSA-168255: Influenza Infection
R-HSA-913531: Interferon Signaling
GO:0034660: ncRNA metabolic process
GO:0045088: regulation of innate immune response
GO:0009615: response to virus
R-HSA-877300: Interferon gamma signaling
GO:0071345: cellular response to cytokine stimulus
GO:0032456: endocytic recycling
R-HSA-6798695: Neutrophil degranulation
GO:1903047: mitotic cell cycle process
M5926: HALLMARK MYC TARGETS V1
GO:0051052: regulation of DNA metabolic process
GO:0000723: telomere maintenance
GO:0065004: protein-DNA complex assembly
GO:0033044: regulation of chromosome organization
CORUM:433: BASC complex (BRCA1-associated genome surveillance complex)
GO:0022613: ribonucleoprotein complex biogenesis
CORUM:1004: RC complex during S-phase of cell cycle
R-HSA-68886: M Phase
GO:0010564: regulation of cell cycle process
hsa04146: Peroxisome
R-HSA-68689: CDC6 association with the ORC:origin complex
R-HSA-1640170: Cell Cycle
GO:0040029: regulation of gene expression, epigenetic
R-HSA-72695: Formation of the ternary complex, and subsequently, the 43S complex
M5928: HALLMARK MYC TARGETS V2
R-HSA-69275: G2/M Transition
GO:0034654: nucleobase-containing compound biosynthetic process
R-HSA-3247509: Chromatin modifying enzymes
R-HSA-2173793: Transcriptional activity of SMAD2/SMAD3:SMAD4 heterotrimer
R-HSA-2559586: DNA Damage/Telomere Stress Induced Senescence
R-HSA-1655829: Regulation of cholesterol biosynthesis by SREBP (SREBF)
R-HSA-68875: Mitotic Prophase
GO:0051095: regulation of helicase activity
GO:0051101: regulation of DNA binding
GO:0033365: protein localization to organelle
GO:1905818: regulation of chromosome separation
R-HSA-9637690: Response of Mtb to phagocytosis
M40: PID E2F PATHWAY
GO:0072344: rescue of stalled ribosome
GO:0000018: regulation of DNA recombination
GO:0062197: cellular response to chemical stress
R-HSA-6796648: TP53 Regulates Transcription of DNA Repair Genes
GO:0016071: mRNA metabolic process
GO:0043687: post-translational protein modification
GO:0061180: mammary gland epithelium development
R-HSA-69017: CDK-mediated phosphorylation and removal of Cdc6
GO:0006513: protein monoubiquitination
R-HSA-2262752: Cellular responses to stress
D
LCMV-Armstrong
LCMV-Clone 13
Ezh2
CD8
50%
83%
CD25
61%
81%
CD44
54%
74%
T-bet
53%
83%
CD44⁺%
CD44 MFI
Ezh2 (MFI)
CD25 (MFI)
Tbet (MFI)
MFI

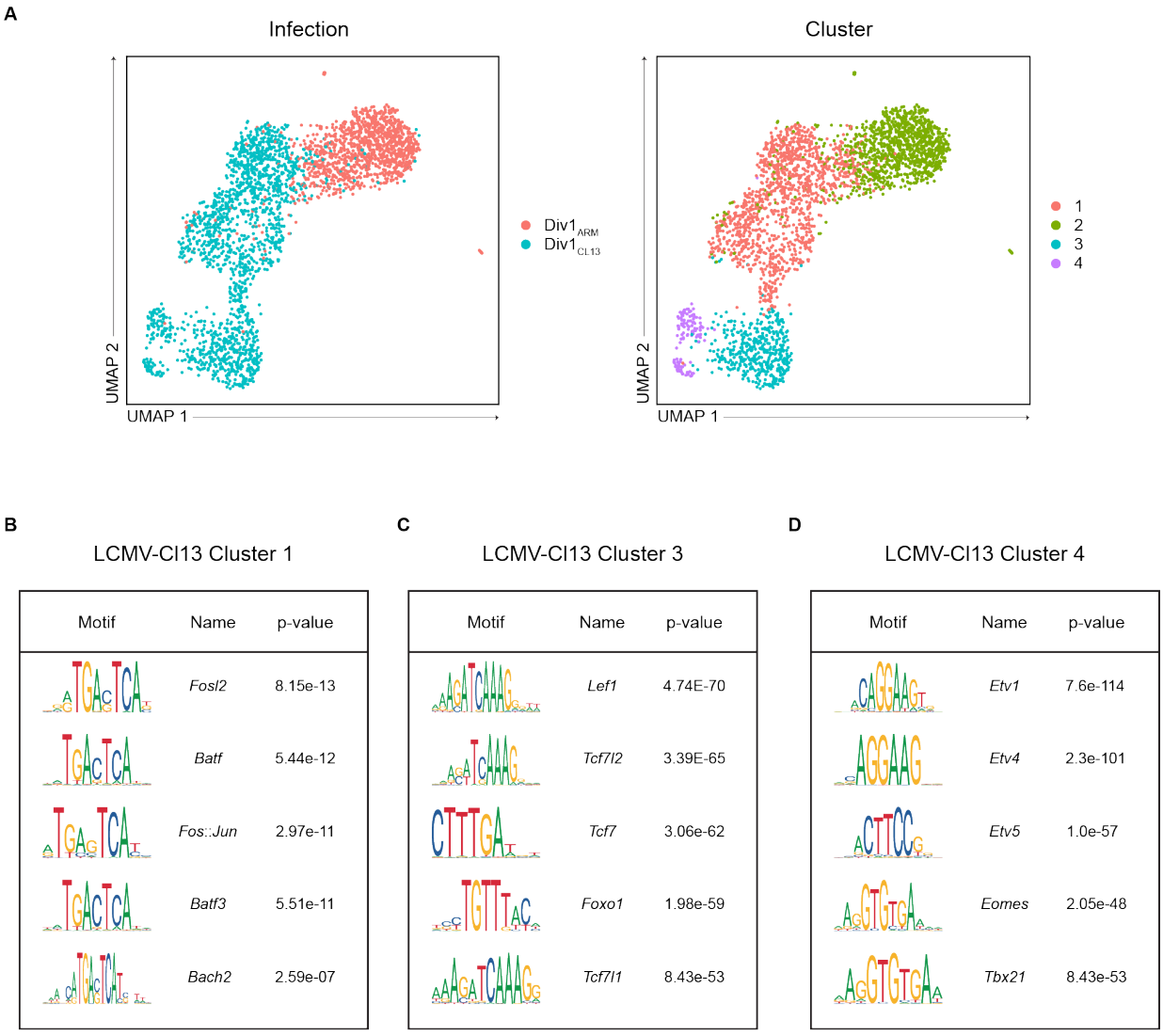

Figure 1.3. CD8⁺ T cells that have undergone their first division in response to LCMV-Arm vs. LCMV-Cl13 exhibit epigenetic and transcriptional dynamics heterogeneity. **(A)** CD8⁺CD45.1⁺ P14 T cells were CSFE-labeled prior to adoptive transfer into separate CD45.2 recipient mice that were infected with either LCMV-Arm vs LCMV-Cl13. Recipient mice were sacrificed at 2 days post-infection and Division 1 (2nd CFSE peak) P14 T cells were FACS-isolated; nuclei were extracted and processed for scATAC-seq using the 10x Genomics pipeline. UMAP clustering of all CD8⁺ cells on the basis of scATAC-seq data colored by infection type (left) or cluster identity (right) is shown. **(B-D)** Selected examples of transcription factor motifs preferentially enriched in accessible chromatin regions from each of the three LCMV-Cl13 clusters.

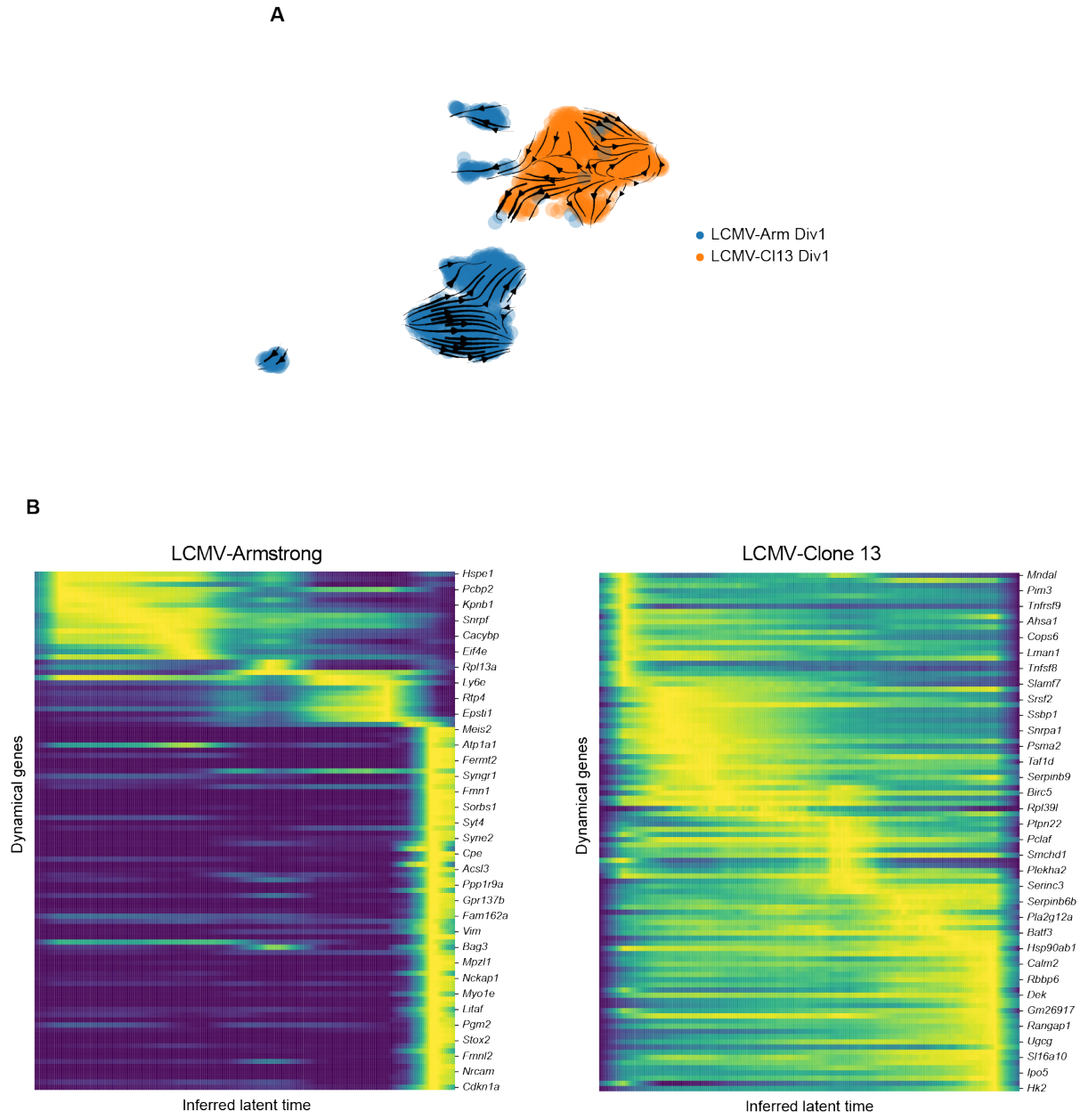

Figure 1.4. CD8⁺ T cells that have undergone their first division in response to LCMV-Arm vs. LCMV-Cl13 exhibit transcriptional dynamics heterogeneity.
(A) RNA velocities of Div1-Arm (blue) and Div1-Cl13 (orange) CD8⁺ T cells derived from scVelo projected onto a UMAP-based embedding. **(B)** Putative driver genes derived from scVelo regulating the CD8⁺ T cell response to LMCV-Arm (left) vs. LCMV-Cl13 (right), represented as heatmaps.

CHAPTER 2: TYPE I INTERFERON MEDIATED EZH2 PLAYS AN EARLY ROLE IN CD8$^+$ T CELL EXHAUSTION THROUGH EPIGENETIC SILENCING

2.1: Introduction

Ezh2 is a component of the PRC2 complex which is a master transcriptional regulator involved in stem cell differentiation and maintenance. In cancer, abnormal expression of PRC2 can result in tumor formation and promotion as disrupting PRC2's activity is deleterious to DNA double strand break repair capability. Ezh2 is the enzymatic component of this complex and is responsible for gene suppression by tri-methylating the lysine at position 27 on histone 3. The effect of Ezh2 modulation in the acute infection context (seen in various viral iterations) has been extensively studied to elicit its role in CD8$^+$ T cell fate and function; less so in the chronic infection or cancer context. Previous studies have shown that modulation of Ezh2 expression is related to tumor health and can be used in conjunction with anti-CTLA4 therapy to enhance its efficacy (Goswami et al. 2018). In Chapter 1 of this dissertation, we discovered that *Ezh2* is upregulated in LCMV-Cl13 infection over LCMV-Arm and that this finding is reflected at the protein level as early as the first division. From this, in Chapter 2, we show that the severity of the exhaustion phenotype, and conversely its rescue, correlates with the level of Ezh2 expression.

Additionally, in the same data set, we found multiple ISGs (e.g. *Isg15*, *Irf4*, *Irf5*, *Ifitm1*, *Irf7*) that are upregulated in CD8$^+$ T cells responding to chronic infection compared to those responding to acute infection. Upon binding of Type I interferons with the Type I interferon receptor (IFNAR), a signaling cascade leading to the potential induction of ~300 ISGs is induced. The expression of these ISGs results in multiple

protective modalities. (Platanias 2022, Marchetti et al. 2006, Sun et al. 2013, Kopitar-Jerala 2017, Lee and Ashkar 2018). Type 1 interferons are cytokines that have a major role in promoting and further regulating the immune response to acute viral infection by upregulating molecules which inhibit viral replication. This family includes 14 variants of IFNα as well as IFNβ, IFNε, IFNκ, IFNω, IFNδ, IFNτ, and IFNζ. Interferon production begins upon pattern recognition receptor (PRR) stimulation and is further amplified by a positive feedback loop initiated by the phosphorylation of IRF7. However, in the context of chronic infection and cancer, Type 1 interferon has previously been shown to promote exhaustion in natural killer cells, plasmacytoid dendritic cells (pDCs), $CD4^+$ Th1 helper cells, and $CD8^+$ T cells (Huang et al. 2021b, TT and EI 2021, Osokine et al. 2014, Snell, McGaha and Brooks 2017) Similarly, upregulation of *Ifnar1* as well as increased expression of its product IFNAR1, results in an exacerbation of the exhaustion phenotype in $CD8^+$ T cells. In this chapter, we find that a reduced expression of *Ifnar1* and neutralization of IFNAR1 function yields a reduction of Ezh2 expression as early as division 1 in LCMV-Cl13 infection. Further, the exhaustion phenotype is rescued in these same conditions at day 5 post-infection. Taken together, these results suggest that IFN-I signaling may play a role in inducing upregulation of Ezh2 in Div1-Cl13 cells, which, in turn, mediates epigenetic repression and contributes to promoting exhaustion.

2.2: Results

2.2.1: Expression of Ezh2 and H3K27me3 is positively correlated and *increased expression of Ezh2 results in an increased expression of exhaustion related molecules*

The observation that the gene encoding Ezh2 was upregulated in $Div1_{Cl13}$ cells (**Figure 1.2B and D**) raised the possibility that epigenetic silencing might be involved in regulating exhaustion. As Ezh2 is responsible for gene suppression by the deposition of tri-methyl groups, we first show the positive correlation of Ezh2 and H3K27me3 expression. We adoptively transferred $CD8^+$ $CD45.1^+$ P14 T cells into $CD45.2^+$ mice which were then infected with either LCMV-Arm or LCMV-Cl13 1 day later. At days 7 and 30 post-infection, spleens were harvested and analyzed by flow cytometry. $CD8^+$ T cells responding to LCMV-Cl13 show an increased expression of both Ezh2 and H3K27 over those responding to LCMV-Arm (**Figure 2.1A**). This result is repeated in the endogenous response where WT mice were similarly infected with LCMV-Arm or LCMV-Cl13 and sacrificed at day 8 or day 30 post-infection (**Figure 2.1B**). The correlation of Ezh2 and H3K27 expression reinforces the known downstream effect of Ezh2 function on suppressive tri-methyl deposition. To investigate how Ezh2 expression level may relate to the expression of exhaustion markers, we further analyzed the flow cytometry results from the adoptive transfer experiment described above. To do this, we gated on Ezh2lo vs Ezh2hi populations in a single host. We find that at day 7 post-infection, Ezh2hi cells also express a higher level of exhaustion markers PD1 and TIM3 as well as TOX, a known driver of exhaustion (**Figure 2.1C**).

2.2.2: Ezh2 mediated genetic silencing regulates exhaustion

To more specifically test the hypothesis that epigenetic silencing might be involved in regulating exhaustion, congenically distinct CD45.1$^+$ control or CD45.1.2$^+$ *Ezh2*$^{fl/fl}$*Cd4*$^{Cre+}$ (Ezh2-deficient) CD8$^+$ P14 T cells were adoptively co-transferred at a 1:1 ratio into CD45.2$^+$ recipients subsequently infected with LCMV-Cl13 and analyzed by flow cytometry 5 days post-infection (**Fig 2.2A**). Compared to control cells, Ezh2-deficient T cells exhibited reduced expression of the exhaustion-associated molecules PD1 and TOX, along with increased expression of TCF1 (**Figure 2.2B, left**); all elements showing a rescue of the exhaustion phenotype. TCF1 increase indicates a rescue of the "stem-like" state of T_{EX}, a decreased likelihood of these cells to progress to terminal exhaustion. Furthermore, Ezh2-deficient T cells exhibited increased expression of Granzyme A, IL-2, and TNF (**Figure 2.2B, right**) indicating a higher level of functionality. Reduction of IL-2 secretion is known to be one of the first functional indications of exhaustion. In terms of inhibitory receptors and transcription factors associated with exhaustion, similar, though abrogated results were observed with Ezh2-heterozygous (Ezh2-HET, *Ezh2*$^{fl/wt}$*Cd4*$^{Cre+}$) CD8$^+$ P14 T cells using the same experimental approach (**Figure 2.2C and 2.2D**). The partial deficiency of Ezh2 in the Ezh2-HET experiment, rather than its complete ablation seen in the Ezh2-KO model, could explain this reduced effect on exhaustion rescue. However, CD8$^+$ T cells from Ezh2-HET mice do not result in a significant increase in IL-2 or TNF secretion as compared to the control cells, indicating a lack of functional rescue. Ezh2, as a known gene repressor, has a broad impact on a variety of cellular processes. Due to this extensive reach in addition to its remaining, though limited, expression in the Ezh2-HET

model, other compensatory signaling pathways may come into play to restore $CD8^+$ T cell secretion of IL-2 and TNF.

In parallel, we asked whether forced expression of Ezh2 might result in increased expression of exhaustion-associated molecules. Congenically distinct $CD8^+$ P14 T cells were transduced with empty vector (EV, $CD45.1^+$) or Ezh2 retroviral constructs (Ezh2 OE, $CD45.1.2^+$), mixed at a 1:1 ratio, and adoptively transferred into $CD45.2^+$ recipients prior to infection with LCMV-Cl13 (**Figure 2.3A**). Compared to control cells, Ezh2 OE $CD8^+$ P14 T cells exhibited increased expression of PD1 and TOX, along with reduced expression of TCF1 and Granzyme A (**Figure 2.3B**). These results are directly opposite of those seen in Ezh2 depletion and reduction and show an exacerbation of exhaustion at D7 post LCMV-Cl13 infection. Taken together, these findings suggest a possible role for Ezh2-mediated epigenetic silencing in regulating exhaustion.

2.2.3: Increased H3K27me3 deposition in $CD8^+$ T cells responding to LCMV-Cl13 compared to those responding to LCMV-Arm

The observation that the gene encoding Ezh2, the enzymatic catalytic subunit of the repressive PRC2 complex, was upregulated in $Div1_{Cl13}$ cells (**Figure 1.2B and D**) raised the possibility that epigenetic silencing might be involved in regulating exhaustion. To further probe this possibility, $CD8^+CD45.1^+$ P14 cells were adoptively transferred into congenically distinct $CD45.2^+$ hosts and infected with either $2x10^5$ PFU LCMV-Arm or $2x10^6$ PFU LCMV-Cl13 the following day. Mice were sacrificed at day 7 post-infection and the donor cells were FACS purified. H3K27me3 and H3K4me3 profiling was then performed with a Cell Signaling CUT&RUN kit and the subsequent

libraries were sequenced and analyzed (**Figure 2.4A**). As the main function of Ezh2 is the deposition of repressive marks on H3K27 and this study has also shown that Ezh2 expression is highly correlated with H3K27 tri-methylation, we used this signal as a proxy to determine Ezh2 binding sites. In LCMV-Cl13 infection, we found 6,538 called peaks (sites of H3K27 tri-methylation), in LCMV-Arm infection, 4,023 peaks and 7,671 peaks were overlapping the two conditions. (**Figure 2.4B**) Enumerating H3K4me3 activating peaks (sites of H3K4 tri-methylation), we found 6,826 peaks in LCMV-Armstrong, 4,167 peaks in LCMV-Cl13, and 8,129 overlapping peaks (**Figure 2.4C**). Consistent with our hypothesis, we observed a higher number of repressive H3K27me3 peaks, but not activating H3K4me3 peaks, in $CD8^+$ T cells responding to LCMV-Cl13 compared to $CD8^+$ T cells responding to LCMV-Arm at day 7 post-infection. Notably, called peaks, sites of H3K27 tri-methylation, were revealed at genes associated with maintenance of effector $CD8^+$ T cells (*Ccl5, Nfatc2*), their cytotoxic functionality (*Il2, Gzmm*), and memory T cells (*Klrg1*) (Crawford et al. 2011, Wherry et al. 2007, Zhu et al. 2022, Chang et al. 2014) in cells from LCMV-Cl13 infected mice and not in those infected with LCMV-Arm. Figure 2.4D illustrates these tracks and specifies the points of peak differentiation. The top blue track shows the peaks in $CD8^+$ T cells responding to LCMV-Arm, the lower red track shows those of LCMV-Cl13 and the diagram of the specified gene is shown on the bottom in purple. Yellow highlights indicate where the called peaks are significantly different from one another indicating sites of H3K27 tri-methylation and further silencing in one infection context versus the other. We also found differences in the overall processes and pathways in these data utilizing gene ontology (GO) analysis. In LCMV-Arm infection, peaks were called within genes

involved in regulation of nitrogen compound, cellular, and organic substance metabolism and catalytic activity (**Figure 2.5A**). However, genes that were differentially methylated could only be meaningfully grouped in very limited areas. On the other hand, in chronic infection, these genes are seen to have much more varied roles in multiple metabolic processes, biosynthetic processes, and transcription regulation (**Figure 2.5B**). Together, these data suggest an epigenetic suppression of processes promoting effective viral clearance and memory formation in $CD8^+$ T cells thus contributing to the exhaustion phenotype.

2.2.4: Type I interferon production is increased in plasmacytoid dendritic cells responding to LCMV-Cl13 infection

Considering the increased expression of interferon stimulated genes (ISGs) in the $Div1_{LCMV\text{-}CL13}$ cluster compared to the $Div1_{ARM}$ clusters (**Figure 1.2B**), we investigated the effect of acute vs. chronic infection on multiple subsets of antigen presenting cells (APCs) and B and T cells. We infected C57BL/6 mice with 2x10^6 pfu LCMV-Arm or LCMV-Cl13 and harvested serum and spleens at day 1 post-infection. Plasmacytoid dendritic cells (pDCs), CD11c hi & CD11c lo dendritic cells, macrophages, B cells, and T cells were FACS isolated and analyzed by qPCR. Among these cell types, we find that pDCs produce a drastically higher amount of Type I interferons, IFNα (**Figure 2.6, left**) and IFNβ (**Figure 2.6, right**) in LCMV-Cl13 vs. LCMV-Arm infection.

2.2.5: Type I interferon signaling may induce Ezh2 expression in CD8$^+$ T cells that have undergone their first division

With the knowledge that ISGs and other genes associated with IFN-I signaling are overexpressed at division 1 in CD8$^+$ T cells responding to chronic infection (**Figure 1.2B**) compared to Div1$_{ARM}$ cells, we asked what factors might mediate Ezh2 upregulation during early response to LCMV-Cl13. This upregulation raised the possibility that IFN-I signaling might regulate Ezh2 expression. We therefore tested whether deletion of IFNAR1, the receptor for IFN-I, in CD8$^+$ T cells might affect Ezh2 expression in Div1 cells. Congenically distinct control *Ifnar*$^{+/+}$ (CD45.1$^+$, IFNAR1-WT) or *Ifnar*$^{-/-}$ (CD45.1.2$^+$, IFNAR1-deficient) CD8$^+$ P14 T cells were labeled with CFSE, mixed at a 1:1 ratio, and adoptively transferred into CD45.2$^+$ recipients prior to infection with LCMV-Cl13 and cells that had undergone their first division (2nd CFSE peak) were analyzed (**Figure 2.7A**). Compared to control cells, IFNAR1-deficient Div1 CD8$^+$ P14 T cells exhibited reduced expression of Ezh2 (**Figure 2.7B**), indicating that IFN-I signaling may mediate upregulation of Ezh2 in CD8$^+$ T cells responding to LCMV-Cl13. We also observed a decrease in the activation markers CD25 and PD1 expression upon IFNAR knockout. Type I interferons are important for initial T cell activation and proliferation, so it follows that knocking out their single receptor then reduces their activation efficiency. Conversely, we found that SLAMF6 expression increased upon IFNAR knockout. SLAMF6, in addition to TCF7, in chronic infection indicates a more “stem-like” state of exhausted T cells which are more prone to rescue by pharmacological means or maintain more effector function (Yigit et al. 2019, Jadhav et al. 2019). Furthermore, at day 5 post-infection, IFNAR1-deficient CD8$^+$ P14 T cells continued to exhibit reduced

Ezh2 expression, along with reduced expression of exhaustion-associated molecules, including PD1, TIM3, and TOX, compared to control cells (**Figure 2.7C**).

Next, we utilized an IFNAR1 neutralizing antibody to investigate the effect of the reduction of function reduction as compared to an isotype control. $CD8^+CD45.1^+$ P14 cells were adoptively transferred to $CD45.2^+$ recipient mice and infected with LCMV-Cl13 1 day later. On day of transfer, infection, and days 2 and 4 post-infection, mice were also treated with either Mouse IgG1 or anti-mouse IFNAR1 blocking antibody. Mice were then sacrificed at day 2 (for division 1 analysis) and day 5 post-infection, their spleens harvested and analyzed by flow cytometry (**Figure 2.8A**). Similar results to those of *Ifnar1* knockout were observed. Ezh2, CD25, and EOMES expression significantly decreased at division 1 in mice treated with anti-IFNAR1 (**Figure 2.8B**). By day 5 post-infection, expression of Ezh2, PD1, TIM3, and TOX were reduced, again indicating exhaustion rescue (**Figure 2.8C**). Overall, these findings suggest a role of IFN-I signaling either by receptor expression or receptor functionality in regulating Ezh2 expression and further $CD8^+$ T cell exhaustion.

2.3: Discussion

Specifically in the context of chronic viral infection, the roles of Ezh2 and Type I interferon are not as well characterized as they are in cancer. Some similarities arise due to the persistent exposure to antigen, which typically connects $CD8^+$ T cell exhaustion in chronic infection and cancer contexts. However, in the context of cancer alone, multiple studies have shown that Ezh2 expression influences the fate of responding $CD8^+$ TILs (tumor infiltrating lymphocytes) and immunotherapeutic CAR

(chimeric antigen receptor) T cells on a case-by-case basis, dependent on biological context. (Chase and Cross 2011, Yoo and Hennighausen 2012, Kang et al. 2020, Weber et al. 2021).

In the previous chapter, we showed that *Ezh2* expression is highly upregulated as early as division 1 in LCMV-Cl13 infection in comparison with LCMV-Arm. Modulating its expression through genetic knockout or knockdown resulted in a rescue of the exhaustion phenotype, shown in a decrease of inhibitory receptors and transcription factors known to be associated with $CD8^+$ T cell exhaustion as early as division 1. This increase in Ezh2 expression also correlates directly with tri-methylation of H3K27 indicating active gene suppression and continues on to later stages of chronic infection. To further investigate which specific genes are being suppressed by H3K27, implicating Ezh2 binding, we used CUT&RUN which is a simpler assay than traditional ChIP-seq but obtains the same goal. We again used an adoptive transfer model with LCMV-Arm vs. LCMV-Cl13 infection to compare the results at day 7. We could not feasibly generate enough T cells upon mouse sacrifice to perform CUT&RUN, so we instead analyzed at day 7 post-infection. We found results anticipated by our hypothesis which stated there are more repressive marks found in $CD8^+$ T cells responding to chronic infection than in acute. GO analysis revealed that a many of these repressive marks found in chronic infection affect transcription regulation and metabolic processes at ay d7.

The next step was to determine whether or not there was an upstream process which would mediate *Ezh2* expression and therefore epigenetic silencing. Amelioration of *Ifnar1* expression by knockout and IFNAR1 function by neutralizing antibody showed

similar results in regulating Ezh2 expression as early as division 1 as well as other markers of activation (CD25), exhausted T cell stem-ness (SLAMF6) and transcription factors known to have an important role in overall T cell differentiation. At division 1, knockout of *Ifnar1* resulted in a decrease of Ezh2, CD25, and PD1 expression and an increase in SLAMF6 expression. Early neutralization of IFNAR function again resulted in a decrease of Ezh2 and CD25 expression. We also observe a decrease in EOMES expression .

Currently, both Type 1 interferon and Ezh2 blockade are being studied as potential combinatorial cancer therapies (Cao et al. 2021, Kang et al. 2020). Our findings provide an impetus to further investigate the effects of these therapies early in the course of detection and treatment of cancer and potentially other chronic infections. The earliest administration possible can potentially abrogate the severity of disease burden further along the time course or perhaps have a more potent effect.

Chapter 2, in full, is an adapted version of the material that has been submitted for publication. Lauren K. Quezada, Wenhao Jin, Yi Chia Liu, Eleanor S. Kim, Zhaoren He, Cynthia S. Indralingam, Tiffani Tysl, Lara Labarta-Bajo, Ellen J. Wehrens, Yeara Jo, Katelynn Kazane, C.J. Hattori, Elina I. Zuniga, Gene W. Yeo, John T. Chang (2022). Early acquisition of phenotypic, transcriptional, and epigenetic features associated with T cell exhaustion. In revision. The dissertation author was primary author of all material.

Figure 2.1. Ezh2 and H3K27me3 expression is positively correlated with indicators of exhaustion

(A) $CD8^+CD45.1^+$ P14 T cells were adoptively transferred into separate CD45.2 recipient mice and were infected with $2x10^5$ PFU LCMV-Arm or $2x10^6$ PFU LCMV-Cl13. Mice were sacrificed 7 and 30 days post-infection and splenocytes analyzed by flow cytometry. Bar graphs indicate the frequencies of Ezh2 (top) and H3K27 (bottom) expression in P14 T cells responding to LCMV-Arm (blue) or LCMV-Cl13 (red) infection. **(B)** WT mice were infected similarly and sacrificed at day 8 and day 30 post-infection. Bar graphs indicate the frequencies of Ezh2 (top) and H3K27 (bottom) expression in responding $gp33^+CD8^+$ T cells. **(C)** Uninfected WT $CD8^+$ T cells (left) provide the Ezh2 gate for $CD8^+CD45.1^+$ P14 T cells harvested at day 7 post-infection, analyzed in (A). Representative flow cytometry plots (left) displaying expression of PD1, TIM3 or TOX among gated donor Ezh2lo or Ezh2hi P14 T cells. Bar graphs indicate the frequencies (middle) or mean fluorescence intensity (MFI, right) of Ezh2lo (blue) or Ezh2hi (red) P14 T cells responding to LCMV-Cl13 *$p < 0.05$, **$p < 0.01$, ***$p < 0.0001$, ****$p < 0.0001$ (paired *t* test). Data are representative of 2 to 3 independent experiments.

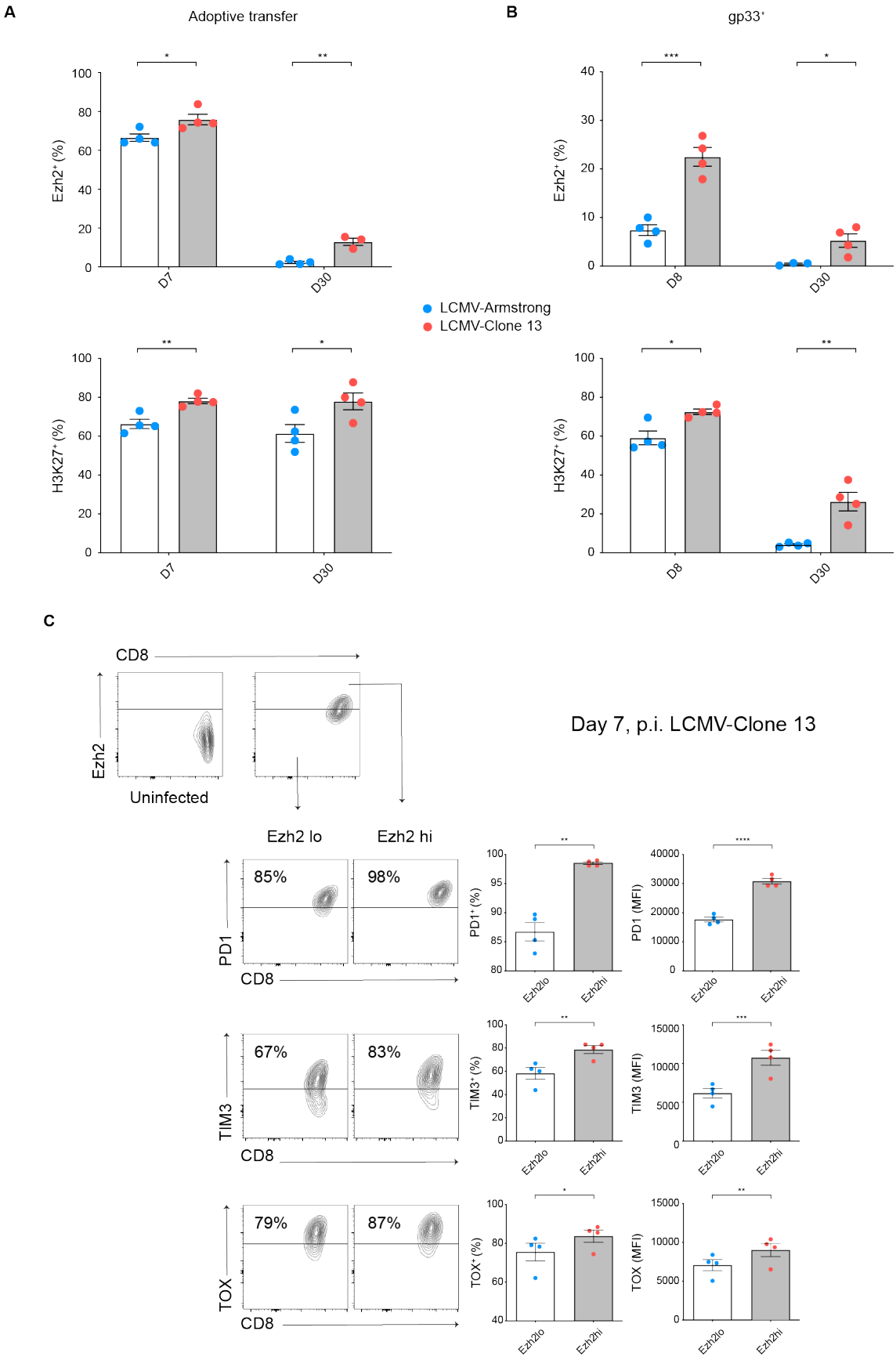
A
Adoptive transfer
B
gp33+
Ezh2+ (%)
H3K27+ (%)
D7
D30
D8
LCMV-Armstrong
LCMV-Clone 13
C
CD8
Ezh2
Uninfected
Day 7, p.i. LCMV-Clone 13
Ezh2 lo
Ezh2 hi
85%
98%
PD1
67%
83%
TIM3
79%
87%
TOX
PD1+ (%)
PD1 (MFI)
TIM3+ (%)
TIM3 (MFI)
TOX+ (%)
TOX (MFI)
Ezh2lo
Ezh2hi

Figure 2.2. Ezh2-mediated epigenetic repression regulates exhaustion rescue. **(A)** Experimental setup. Control CD45.1$^+$ (wild-type, WT) and Ezh2-deficient CD45.1.2$^+$(*Ezh2*$^{fl/fl}$*Cd4*$^{Cre+}$*,* Ezh2 KO) CD8$^+$ P14 T cells were co-transferred into congenically distinct CD45.2$^+$ recipient mice prior to infection with LCMV-Cl13; recipient mice were sacrificed at 5-7 days post-infection and splenocytes analyzed by flow cytometry. **(B)** Representative flow cytometry plots (left) displaying expression of PD1, TCF1, TOX, Granzyme A, IL-2, or TNF protein among gated donor WT or Ezh2 KO P14 T cells. Bar graphs indicate the frequencies (middle) or mean fluorescence intensity (MFI, right) of WT (blue) or Ezh2 KO (red) P14 T cells responding to LCMV-Cl13 **(C)** Control CD45.1$^+$ (wild-type, WT) and Ezh2-heterozygous CD45.1.2$^+$*(Ezh2*$^{fl/wt}$*Cd4*$^{Cre+}$*,* Ezh2 HET) CD8$^+$ P14 T cells were co-transferred into congenically distinct CD45.2$^+$ recipient mice prior to infection with LCMV-Cl13; recipient mice were sacrificed at 5-7 days post-infection and splenocytes analyzed by flow cytometry. **(D)** Representative flow cytometry plots (left) displaying expression of PD1, TCF1, TOX, or Granzyme A protein among gated donor WT or Ezh2 HET P14 T cells. Bar graphs indicate the frequencies (middle) or mean fluorescence intensity (MFI, right) of WT (blue) or Ezh2 HET (red) P14 T cells responding to LCMV-Cl13. Data are shown as mean ± SEM. *p < 0.05, **p < 0.01, ***p < 0.0001, ****p < 0.0001 (paired t test). Data are representative of 2 to 3 independent experiments.

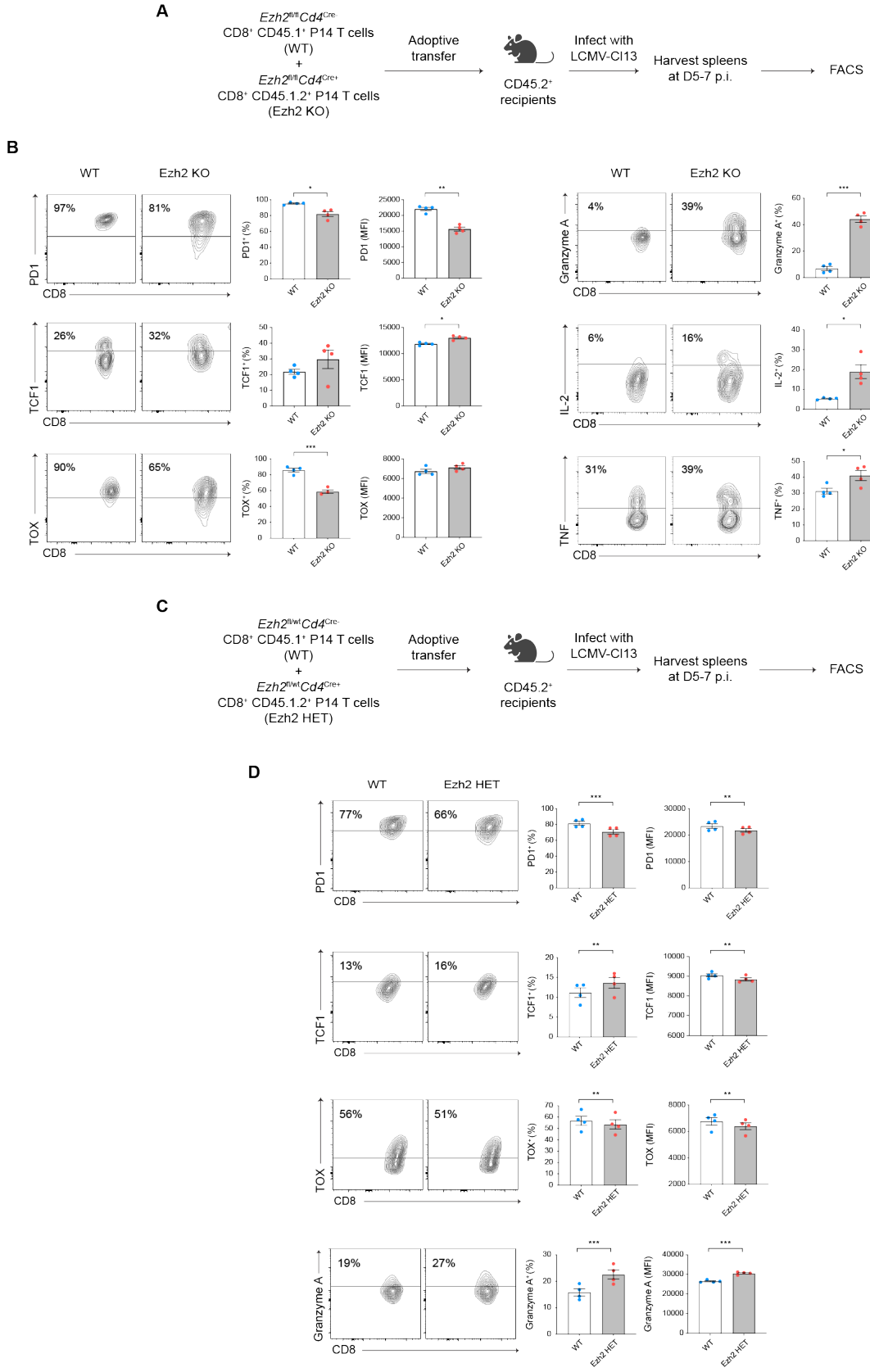
A
Ezh2fl/fl Cd4Cre-
CD8+ CD45.1+ P14 T cells
(WT)
+
Ezh2fl/fl Cd4Cre+
CD8+ CD45.1.2+ P14 T cells
(Ezh2 KO)
Adoptive transfer
CD45.2+ recipients
Infect with LCMV-Cl13
Harvest spleens at D5-7 p.i.
FACS
B
WT
Ezh2 KO
PD1
CD8
97%
81%
PD1+ (%)
PD1 (MFI)
TCF1
26%
32%
TCF1+ (%)
TCF1 (MFI)
TOX
90%
65%
TOX+ (%)
TOX (MFI)
Granzyme A
4%
39%
Granzyme A+ (%)
Granzyme A (MFI)
IL-2
6%
16%
IL-2+ (%)
IL-2 (MFI)
TNF
31%
39%
TNF+ (%)
TNF (MFI)
C
Ezh2fl/wt Cd4Cre-
CD8+ CD45.1+ P14 T cells
(WT)
+
Ezh2fl/wt Cd4Cre+
CD8+ CD45.1.2+ P14 T cells
(Ezh2 HET)
Adoptive transfer
CD45.2+ recipients
Infect with LCMV-Cl13
Harvest spleens at D5-7 p.i.
FACS
D
WT
Ezh2 HET
PD1
CD8
77%
66%
PD1+ (%)
PD1 (MFI)
TCF1
13%
16%
TCF1+ (%)
TCF1 (MFI)
TOX
56%
51%
TOX+ (%)
TOX (MFI)
Granzyme A
19%
27%
Granzyme A+ (%)
Granzyme A (MFI)

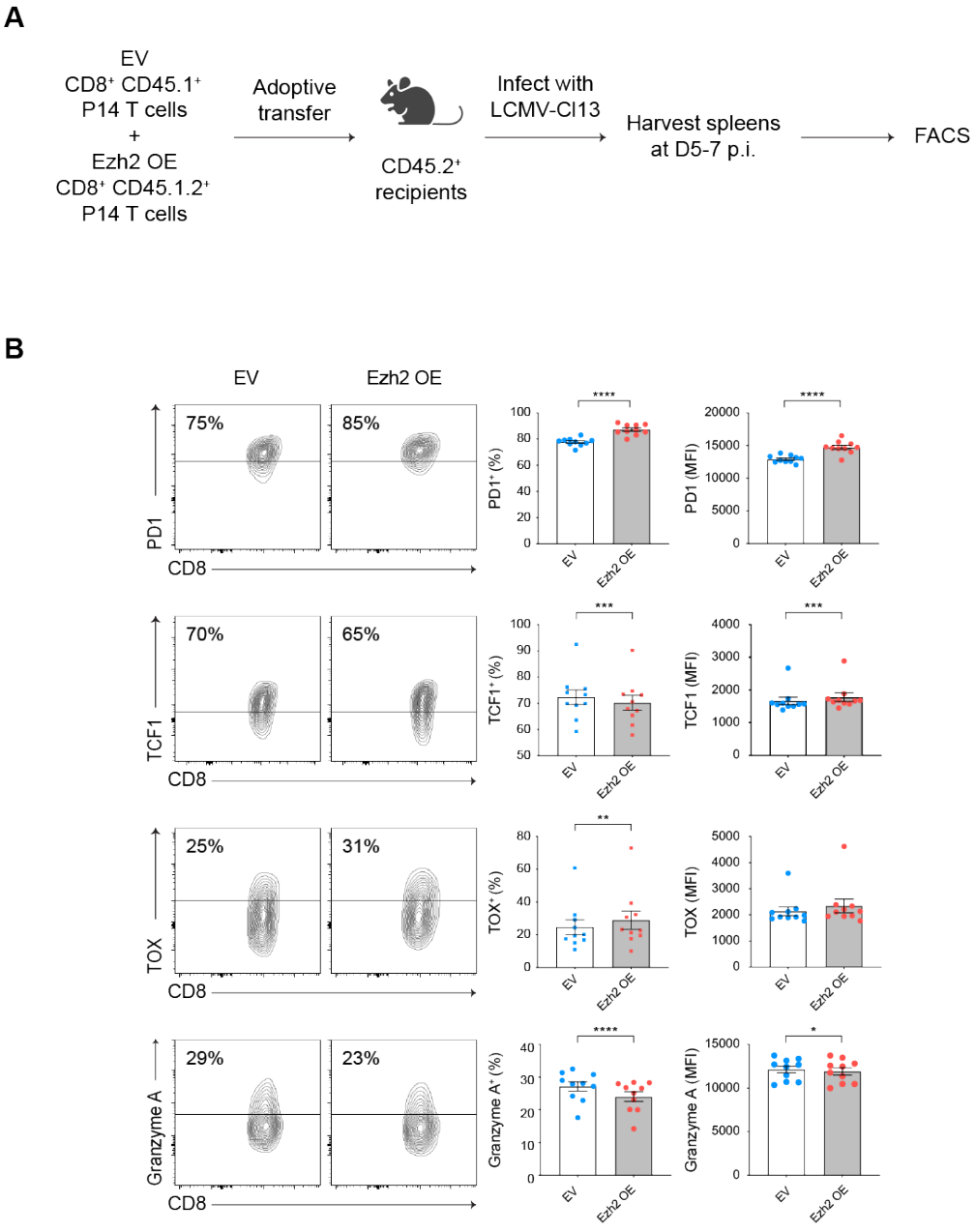

Figure 2.3. Ezh2 overexpression exacerbates the exhaustion phenotype.
(A) Experimental setup. CD8$^+$ P14 T cells were transduced with an empty vector control (EV, CD45.1$^+$) or Ezh2 overexpression (Ezh2-OE, CD45.1.2$^+$) construct prior to adoptive cotransfer into CD45.2$^+$ recipient mice prior to infection with LCMV-Cl13; recipient mice were sacrificed at 5-7 days post-infection and splenocytes analyzed by flow cytometry. **(B)** Representative flow cytometry plots (left) displaying expression of PD1, TCF1, TOX, and Granzyme A among gated donor EV or Ezh2-OE P14 T cells. Bar graphs indicate the frequencies (middle) or mean fluorescence intensity (MFI, right) of EV (blue) or Ezh2-OE (red) P14 T cells expressing each molecule.

Figure 2.4 Increased H3K27me3 deposition in $CD8^+$ T cells responding to LCMV-Cl13 compared to those responding to LCMV-Arm. (A) Experimental setup. $CD8^+CD45.1^+$ P14 T cells were harvested from WT mice and adoptively transferred into recipient mice and infected with $2x10^5$ PFU LCMV-ARM or $2x10^6$ PFU LCMV-Cl13 1 day later. Mice sacrificed at day 7 post-infection, spleens harvested and donor cells FACS purified. A Cell Signaling CUT&RUN kit (#86652) was then used for H3K27me3 profiling per manufacturer's instructions. Libraries were sequenced and analyzed. **(B, C)** Venn diagram analysis of shared and differential H3K27me3 (B) or H3K4me3 (C) peaks identified in accessible chromatin regions from $CD8^+$ T cells responding to LCMV-Arm vs. LCMV-Cl13. **(D)** LCMV-Arm (top, blue) and LCMV-Cl13 (bottom, red) tracks indicating peaks (sites) of H3K27 tri-methylation at *Ccl5, Klrg1, Il2, Nfatc2*, and *Gzmm*.

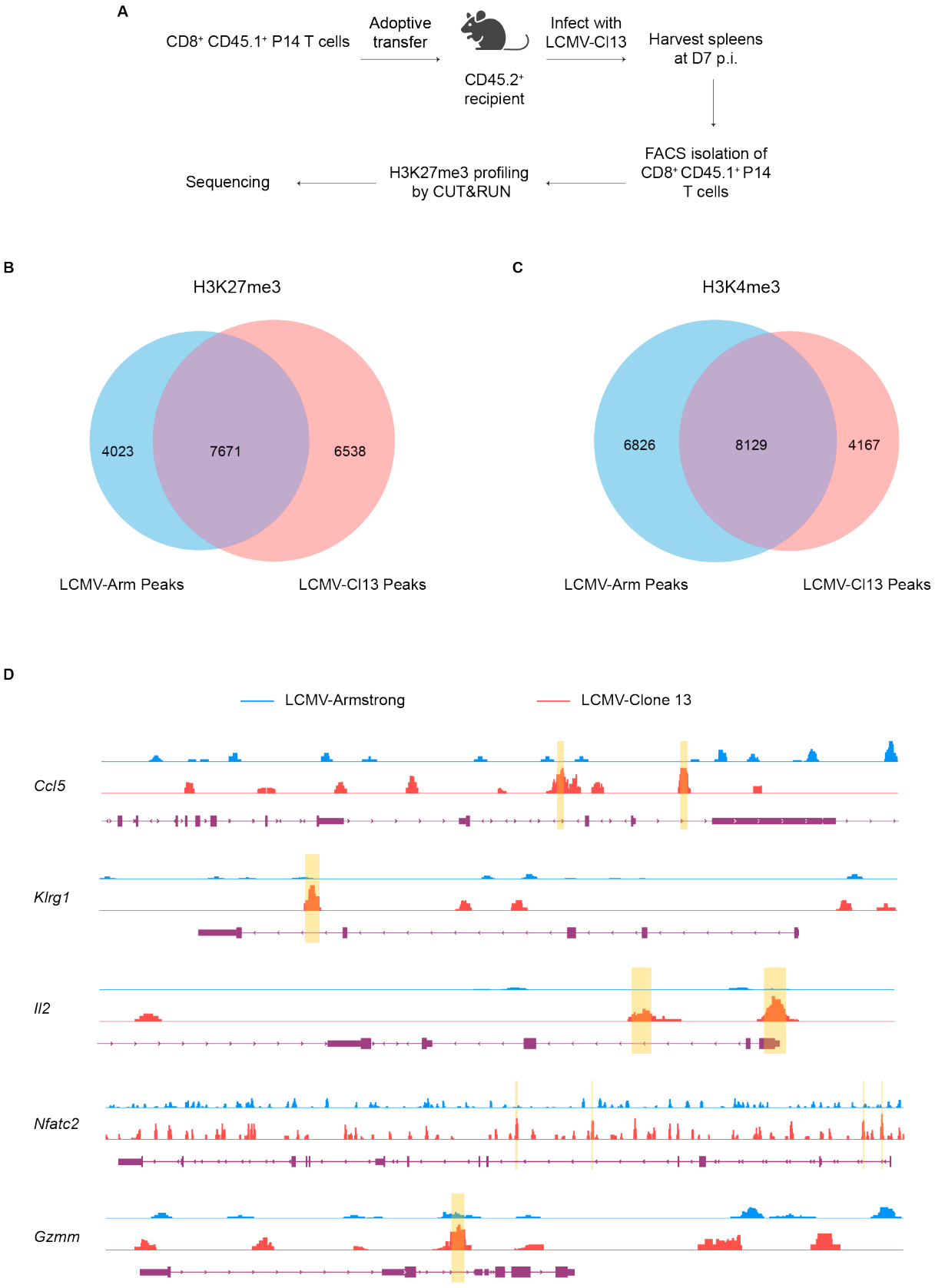
A
CD8⁺ CD45.1⁺ P14 T cells
Adoptive transfer
CD45.2⁺ recipient
Infect with LCMV-Cl13
Harvest spleens at D7 p.i.
FACS isolation of CD8⁺ CD45.1⁺ P14 T cells
H3K27me3 profiling by CUT&RUN
Sequencing
B
H3K27me3
4023
7671
6538
LCMV-Arm Peaks
LCMV-Cl13 Peaks
C
H3K4me3
6826
8129
4167
LCMV-Arm Peaks
LCMV-Cl13 Peaks
D
LCMV-Armstrong
LCMV-Clone 13
Ccl5
Klrg1
Il2
Nfatc2
Gzmm

Figure 2.5 Differential sites of H3K27 tri-methylation in CD8$^+$ T cells in acute and chronic infection have distinct profiles of processes and pathways by GO analysis Called peaks indicate sites of gene silencing due to H3K27 tri-methyl deposition. GO analysis groups these silenced genes (peaks) into categories of processes and pathways as seen in the (**A)** LCMV-Arm context and the **(B)** LCMV-Cl13 context

A

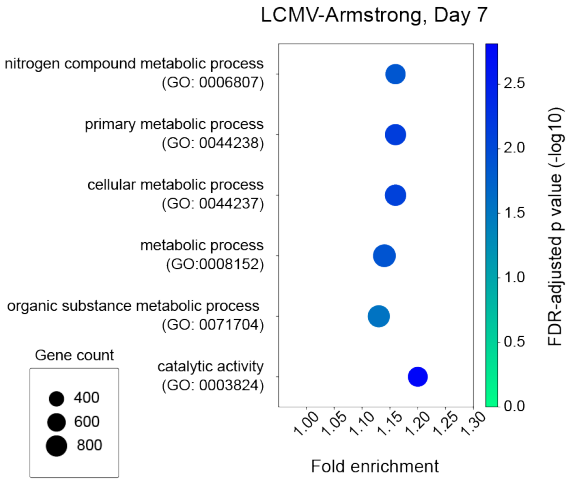
LCMV-Armstrong, Day 7
nitrogen compound metabolic process (GO: 0006807)
primary metabolic process (GO: 0044238)
cellular metabolic process (GO: 0044237)
metabolic process (GO:0008152)
organic substance metabolic process (GO: 0071704)
catalytic activity (GO: 0003824)
Gene count
400
600
800
1.00
1.05
1.10
1.15
1.20
1.25
1.30
Fold enrichment
2.5
2.0
1.5
1.0
0.5
0.0
FDR-adjusted p value (-log10)

B

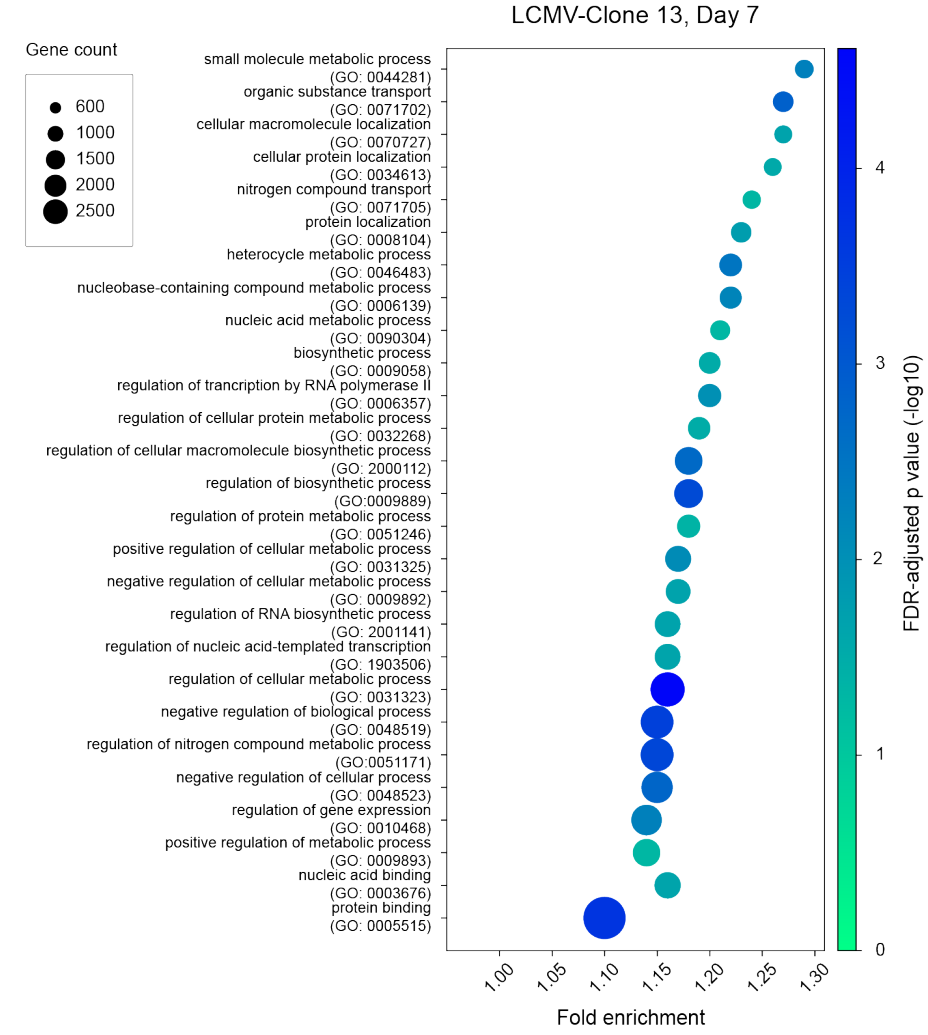
LCMV-Clone 13, Day 7
Gene count
600
1000
1500
2000
2500
small molecule metabolic process (GO: 0044281)
organic substance transport (GO: 0071702)
cellular macromolecule localization (GO: 0070727)
cellular protein localization (GO: 0034613)
nitrogen compound transport (GO: 0071705)
protein localization (GO: 0008104)
heterocycle metabolic process (GO: 0046483)
nucleobase-containing compound metabolic process (GO: 0006139)
nucleic acid metabolic process (GO: 0090304)
biosynthetic process (GO: 0009058)
regulation of trancription by RNA polymerase II (GO: 0006357)
regulation of cellular protein metabolic process (GO: 0032268)
regulation of cellular macromolecule biosynthetic process (GO: 2000112)
regulation of biosynthetic process (GO:0009889)
regulation of protein metabolic process (GO: 0051246)
positive regulation of cellular metabolic process (GO: 0031325)
negative regulation of cellular metabolic process (GO: 0009892)
regulation of RNA biosynthetic process (GO: 2001141)
regulation of nucleic acid-templated transcription (GO: 1903506)
regulation of cellular metabolic process (GO: 0031323)
negative regulation of biological process (GO: 0048519)
regulation of nitrogen compound metabolic process (GO:0051171)
negative regulation of cellular process (GO: 0048523)
regulation of gene expression (GO: 0010468)
positive regulation of metabolic process (GO: 0009893)
nucleic acid binding (GO: 0003676)
protein binding (GO: 0005515)
1.00
1.05
1.10
1.15
1.20
1.25
1.30
Fold enrichment
4
3
2
1
0
FDR-adjusted p value (-log10)

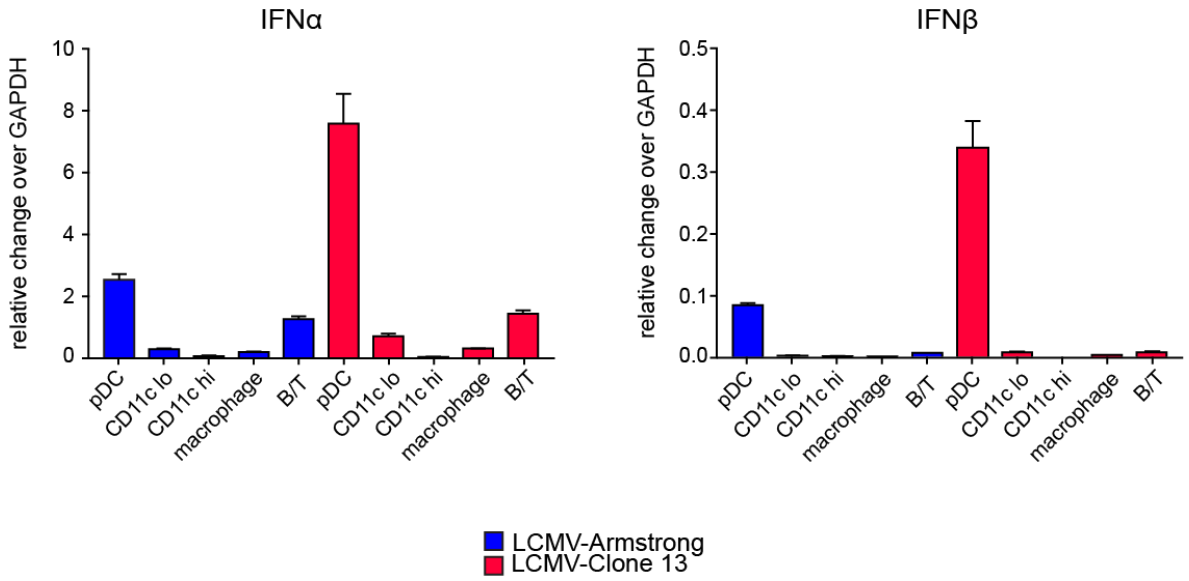

Figure 2.6. Elevated levels of Type 1 interferon are secreted by pDCs in chronic vs acute infection

WT mice were infected with either $2x10^6$ PFU LCMV-Cl13 or LCMV-Arm intravenously and sacrificed on day 2 post-infection. pDC, CD11clo, CD11chi, macrophages, B/T cells were FACS purified and RNA transcripts quantified by qRT-PCR. The relative transcript amounts were normalized against murine *Gapdh*. Data are representative of technical triplicates of one representative experiment.

Figure 2.7. Type 1 interferon may play a role in regulating Ezh2 expression and the exhaustion phenotype at the first division

(A) Control CD45.1$^+$ (*Ifnar*$^{+/+}$ wild-type, WT) and IFNAR1-deficient CD45.1.2$^+$(*Ifnar1*$^{-/-}$, IFNAR1 KO) CD8$^+$ P14 T cells were labeled with CFSE (B only) and co-transferred into congenically distinct CD45.2$^+$ recipient mice prior to infection with LCMV-Cl13; recipient mice were sacrificed at 2 (B) or 5 days (C) post-infection and splenocytes analyzed by flow cytometry. **(B)** Representative flow cytometry plots (left) displaying expression of Ezh2, CD25, PD1, and SLAMF6 protein among gated Division 1 (2nd CFSE peak) WT vs. IFNAR1 KO P14 T cells. Bar graphs indicate the frequencies (middle) or mean fluorescence intensity (MFI, right) of WT (blue) or IFNAR1 KO (red) P14 T cells expressing each molecule. **(C)** Representative flow cytometry plots (left) displaying expression of Ezh2, PD1, TIM3, and TOX protein among gated WT vs. IFNAR1 KO P14 T cells. Bar graphs indicate the frequencies (middle) or mean fluorescence intensity (MFI, right) of WT (blue) or IFNAR1 KO (red) P14 T cells expressing each molecule. Data are shown as mean ± SEM. *$p < 0.05$, **$p < 0.01$, ***$p < 0.0001$, ****$p < 0.0001$ (paired *t* test). Data are representative of 2 to 3 independent experiments.

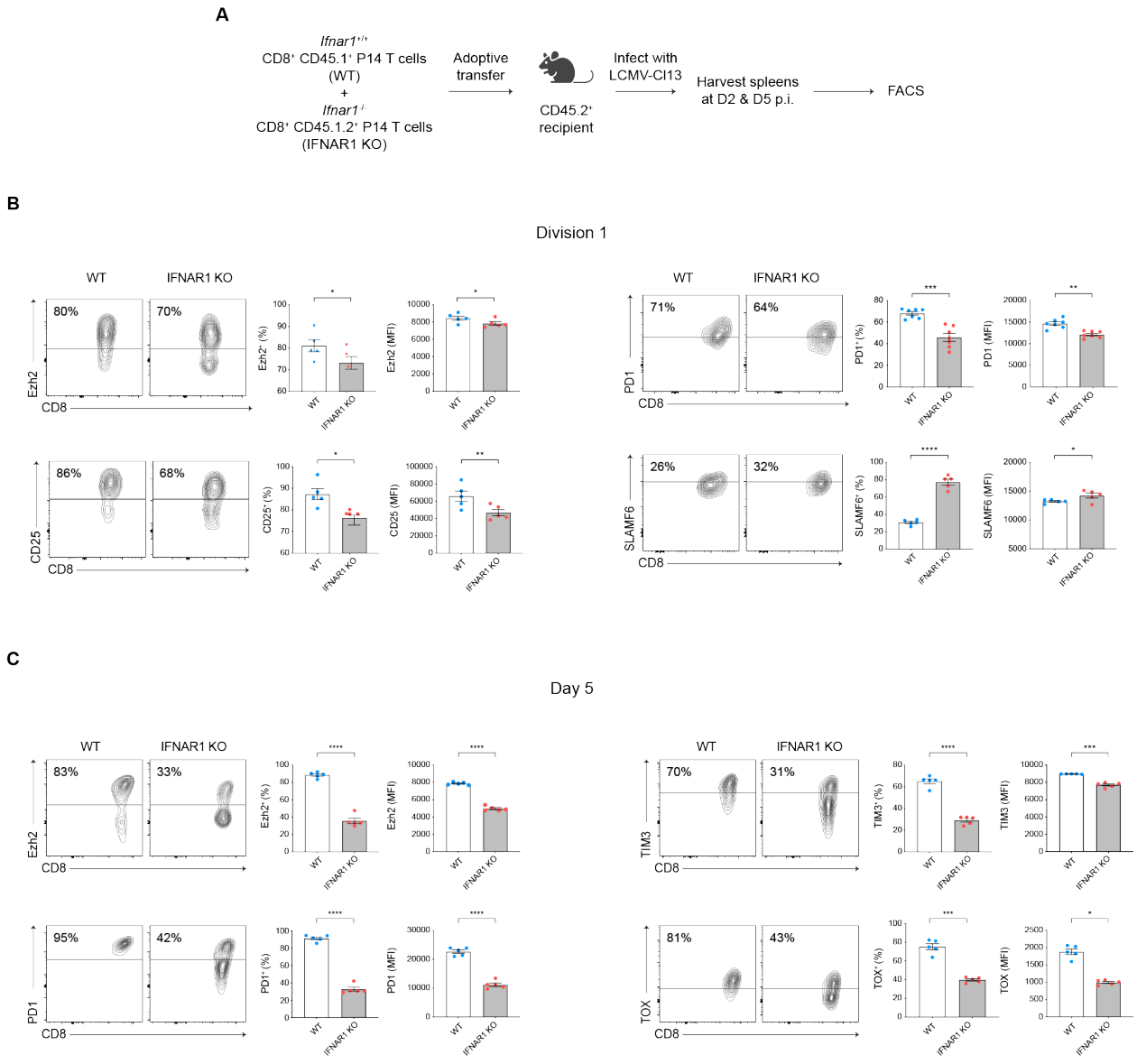
A
Ifnar1+/+
CD8+ CD45.1+ P14 T cells
(WT)
+
Ifnar1-/-
CD8+ CD45.1.2+ P14 T cells
(IFNAR1 KO)
Adoptive transfer
CD45.2+ recipient
Infect with LCMV-Cl13
Harvest spleens at D2 & D5 p.i.
FACS
B
Division 1
WT
IFNAR1 KO
80%
70%
Ezh2
CD8
Ezh2+ (%)
Ezh2 (MFI)
86%
68%
CD25
CD25+ (%)
CD25 (MFI)
71%
64%
PD1
PD1+ (%)
PD1 (MFI)
26%
32%
SLAMF6
SLAMF6+ (%)
SLAMF6 (MFI)
C
Day 5
83%
33%
95%
42%
70%
31%
TIM3
TIM3+ (%)
TIM3 (MFI)
81%
43%
TOX
TOX+ (%)
TOX (MFI)

Figure 2.8. Type I interferon signaling may induce Ezh2 expression in CD8$^+$ T cells that have undergone their first division. (A) CD45.1$^+$ or CD45.1.2$^+$ P14 T cells were transferred into separate CD45.2 recipient mice prior to infection with LCMV-Cl13. For analysis of Division 1 cells, P14 cells were labeled with CFSE prior to transfer. Mice were treated with control isotype mAbs (CD45.1$^+$) or anti-IFNAR1 blocking (CD45.1.2$^+$) mAbs on the day of infection (day 0). For analysis performed at day 5 post-infection, antibodies were also administered on days 2 and 4 post-infection. Mice were sacrificed on day 2 or 5 post-infection for flow cytometry analysis. **(B)** Representative flow cytometry plots (left) displaying expression of Ezh2, CD25 and EOMES protein among gated Division 1 (2nd CFSE peak) isotype- vs anti-IFNAR1-treated P14 T cells. Bar graphs indicate the frequencies (middle) or mean fluorescence intensity (MFI, right) of isotype- (blue) or anti-IFNAR1-treated (red) P14 T cells expressing Ezh2. **(C)** Representative flow cytometry plots (left) displaying expression of Ezh2, PD1, TIM3, and TOX protein among isotype- vs anti-IFNAR-treated P14 T cells. Bar graphs indicate the frequencies (middle) or mean fluorescence intensity (MFI, right) of isotype- (blue) or anti-IFNAR-treated (red) P14 T cells expressing each molecule. Data are shown as mean $\pm$ SEM. *$p < 0.05$, **$p < 0.01$, ***$p < 0.0001$, ****$p < 0.0001$ (Student's t test). Data are representative of 2 to 3 independent experiments.

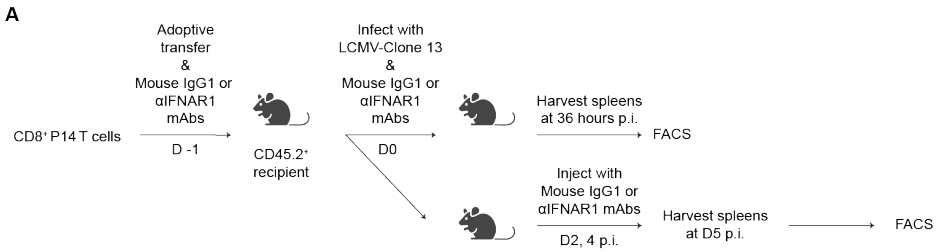
A
CD8+ P14 T cells
Adoptive transfer & Mouse IgG1 or αIFNAR1 mAbs
D -1
CD45.2+ recipient
Infect with LCMV-Clone 13 & Mouse IgG1 or αIFNAR1 mAbs
D0
Harvest spleens at 36 hours p.i.
FACS
Inject with Mouse IgG1 or αIFNAR1 mAbs
D2, 4 p.i.
Harvest spleens at D5 p.i.
FACS

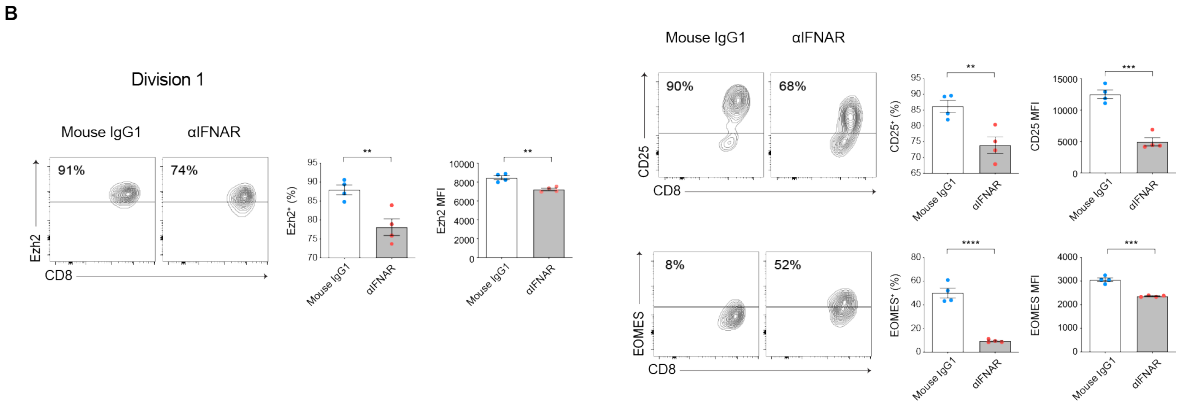
B
Division 1
Mouse IgG1
αIFNAR
91%
74%
Ezh2
CD8
Ezh2+ (%)
Ezh2 MFI
Mouse IgG1
αIFNAR
90%
68%
CD25
CD25+ (%)
CD25 MFI
8%
52%
EOMES
EOMES+ (%)
EOMES MFI

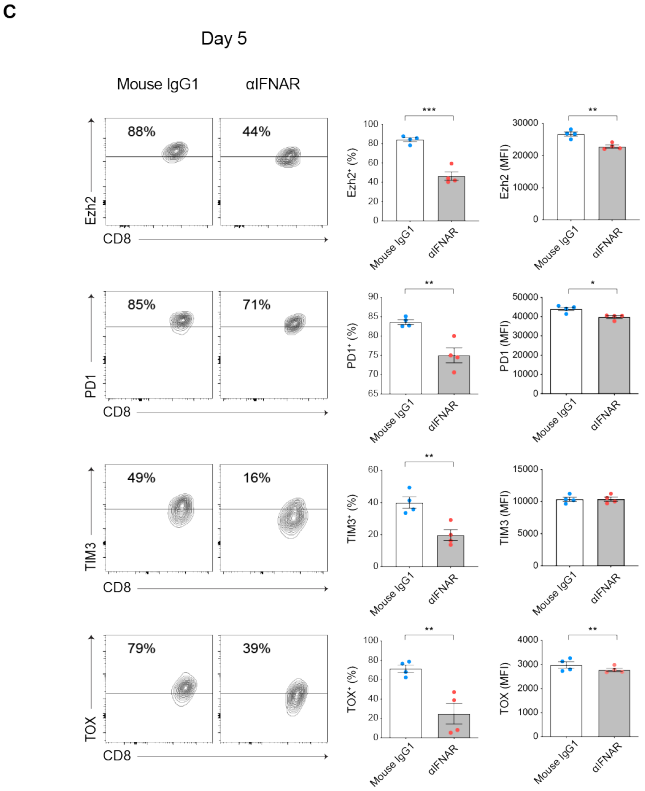
C
Day 5
Mouse IgG1
αIFNAR
88%
44%
Ezh2
CD8
Ezh2+ (%)
Ezh2 (MFI)
85%
71%
PD1
PD1+ (%)
PD1 (MFI)
49%
16%
TIM3
TIM3+ (%)
TIM3 (MFI)
79%
39%
TOX
TOX+ (%)
TOX (MFI)

CHAPTER 3: CONCLUSION

Although substantial progress has been made in elucidating the transcriptional and epigenetic regulation of exhaustion, the precise sequence of events controlling the formation of T_{EX} cells remains incompletely understood. In particular, from what precursor cells are T_{EX} cells derived? It was initially thought that T_{EX} cells were derived from terminally differentiated effector cells. However, lineage tracing experiments demonstrated that $CD127^{hi}KLRG1^{lo}$ memory precursor T cells, but not $KLRG1^{hi}$ effector T cells, can give rise to T_{EX} cells (Angelosanto et al. 2012). More recent studies have shown a much earlier divergence of $CD8^+$ T cell fate in acute vs. chronic infection. By multiple single cell sequencing studies, such transcription factors as TOX, BATF and IRF4 have been determined to drive exhaustion as early as day 4.5 post-infection, while earlier studies typically began their interrogations about 8 days post-infection (Yao et al. 2019, Khan et al. 2019, Seo et al. 2021, K et al. 2017, Chen et al. 2021). Probing deeper into the ontogeny of exhausted T cells, studies have further defined progenitor and intermediate subsets based on high expression of molecules such as TCF1, CXCR5, SLAMF6, and T-bet. More terminally exhausted T cells are defined by sustained expression of the inhibitory receptors PD1 and TIM3 as well as high expression of CD101, CX3CR1, TOX, and EOMES (Yi, Cox and Zajac 2010, Wherry and Kurachi 2015, Hudson et al. 2019, Beltra et al. 2020). In this dissertation we utilized scRNA-seq to similarly interrogate the differences between $CD8^+$ T cells responding to acute vs. chronic infection across an extensive timecourse. Transcriptionally, we found that the T cells responding to LCMV-Arm, as expected, formed two distinct clusters each reflecting gene expression patterns similar to either memory precursor or terminal effector cells ($Div1_{ARM\text{-}MEM}$ and

$Div1_{ARM\text{-}EFF}$ respectively) at division 1. Strikingly, cells responding to LCMV-Cl13 ($Div1_{CL13}$) clustered separately from LCMV-Arm and lost this heterogeneity, forming only one homogeneous cluster. Differential gene analysis showed an upregulation of transcription factors, ISGs and exhaustion associated molecules in $Div1_{CL13}$ over both $Div1_{ARM}$ clusters. In addition to distinctions in the transcriptional landscape, epigenetic differences further distinguish T cells responding to acute and chronic infection.

It is now evident that T_{EX} cells are a distinct subset of $CD8^+$ T cells that differ from effector and memory T cells by ~6,000 open chromatin regions (Mognol et al. 2017, Pauken et al. 2016, M et al. 2017, DR et al. 2016). This epigenetic divergence is evident by day 5 post-infection and becomes progressively more widespread and permanent with time, resulting in durable epigenetic 'scars' (Abdel-Hakeem et al. 2021). Further, these 'scars' are also evident in humans. ATAC-seq was performed on samples from patients with Hepatitis C (HCV) before and after treatment and cure. ChARs (chromatin accessible regions) retained after cure were considered "exhaustion-specific" and found at exhaustion related genes such as *BATF*, *ENTPD1*, and *NFAT* indicating that the epigenetic plasticity of exhausted $CD8^+$ T cells is very limited (KB et al. 2021). Our observation that $CD8^+$ T cells that have undergone their first division in response to LCMV-Arm vs. LCMV-Cl13 exhibit heterogeneity on the basis of their chromatin accessibility patterns suggests the possibility that epigenetic changes may begin to occur earlier than previously appreciated. Of note, heterogeneity was found in the epigenetic landscape of cells responding to LCMV-Cl13 but not in LCMV-Arm in contrast to the transcriptional pattern of LCMV-Arm displaying heterogeneity and not LCMV-Cl13. Interrogating the differences of preferentially enriched transcription factor

motifs between the three clusters generated in scATAC-seq analysis may provide additional insight into functional differences of these clusters.

Additionally, in light of prior data showing that restimulated $CD8^+$ T cells FACS-isolated 30 days after LCMV-Cl13 infection exhibited a reduced capacity to undergo asymmetric cell division (M et al. 2019), which has been shown to result in differentially fated progeny during acute infection (Chang et al. 2007, JT et al. 2011), it is intriguing to speculate that formation of the transcriptionally homogenous $Div1_{CL13}$ population may result, in part, from an impaired capability to undergo asymmetric division. Future studies will investigate this possibility as well as the transcriptional and epigenetic changes following the first $CD8^+$ T cell division in response to LCMV-Cl13.

With regard to the specific epigenetic changes that regulate exhaustion, several prior reports have suggested a role for epigenetic silencing, analogous to its role in terminal effector cell differentiation, in which Ezh2 mediates repression of genes associated with memory cell differentiation (Kakaradov et al. 2017, SM et al. 2017). For example, application of an integrative network modeling approach suggested that epigenetic silencing mediated by Ezh2 may play a role in regulating exhaustion (Bolouri et al. 2020). Furthermore, the microRNA miR-155 increased $CD8^+$ T cell anti-tumor function by restraining T cell senescence and functional exhaustion through PRC2-mediated epigenetic silencing of transcription factors driving terminal differentiation and exhaustion (Ji et al. 2019). Consistent with these results, we observed that at day 7 post-infection, $CD8^+$ T cells responding to LCMV-Cl13 exhibited increased H3K27me3 repressive marks compared to $CD8^+$ T cells responding to LCMV-Arm. Furthermore, Ezh2

deficiency resulted in reduced expression of exhaustion-associated molecules by $CD8^+$ T cells responding to LCMV-Cl13, whereas forced Ezh2 expression resulted in increased expression, supporting the hypothesis that epigenetic silencing may play a critical role in the molecular regulation of exhaustion. In addition, our data suggest that responsiveness to IFN-I signaling may be involved in the initial upregulation of Ezh2 in $CD8^+$ T cells responding to LCMV-Cl13. Future studies will focus on identifying the cellular sources of IFN-I that induce Ezh2 expression and favor early T_{EX} differentiation as well as elucidating the timing and mechanisms by which epigenetic silencing results in acquisition of an early T_{EX} cell state. Our demonstration of the earliest diversion of chronic infection seen thus far, can inform future studies probing specific genes specified in our single cell datasets, adding to the body of evidence defining the ontogeny and progression of T_{EX}. Taken together, these findings suggest the possibility that $CD8^+$ T cells responding to LCMV-Cl13 may enter a pre-exhausted precursor state soon after activation, thus bypassing a functional effector intermediate state.

APPENDIX A: MATERIALS AND METHODS

Mice

All mice were housed under specific pathogen–free conditions in an American Association of Laboratory Animal Care–approved facility at UCSD, and all procedures were approved by the UCSD Institutional Animal Care and Use Committee. C57BL6/J (CD45.1.2$^+$ or CD45.2$^+$) and P14 TCR transgenic (CD45.1$^+$ or CD45.1.2$^+$, maintained on a C57BL6/J background) mice were bred at UCSD or purchased from the Jackson Laboratories. Recipient male and donor female mice used in adoptive transfer experiments were all 6 to 9 weeks of age. No randomization of blinding was used in infection experiments and only mice that had rejected adoptively transferred P14 CD8$^+$ T cells were excluded.

Antibodies, flow cytometry, and cell sorting

Cells were stained for 15 minutes on ice with the following antibodies: Vβ8.1/8.2 (MR5-2), CD8α (53-6.7), CD45.1 (A20), CD45.2 (104), Ezh2 (11/Ezh2), H3K27me3 (C36B11), PD1 (29F.1A12), TIM3 (RMT3-23), CD25 (PC61), CD44 (IM7), TOX (REA473), SLAMF6 (330-AJ), EOMES (Dan11mag), TCF1 (6444S), and Granzyme A (3G8.5). TCF1 and H3K27me3 were purchased from Cell Signaling Technology, TOX from Miltenyi Biotec, Granzyme A from Thermo Fisher Scientific and the remainder from Biolegend. Samples were then stained with Fixable Viability Dye eFluor780 (Thermo Fisher Scientific), for 15 minutes on ice. For all intracellular stains, cells were fixed in either 2% paraformaldehyde or fixed and permeabilized with the FoxP3/Transcription Factor Staining Buffer Kit (Thermo Fisher Scientific). For analysis, all samples were run

on an Accuri C6, LSRFortessa X-20 (BD Biosciences) or Novocyte (Agilent Biosciences). For sorting, all samples were run on an Influx, FACSAria Fusion or FACSAria2 (BD Biosciences). BD FACS DIVA (BD Biosciences) or NovoExpress (Agilent Biosciences) software was used for data collection and FlowJo software (BD Biosciences) was used for analysis of flow cytometry data.

In vivo mouse experiments

Splenocytes were collected from naïve CD45.1$^+$ or CD45.1.2$^+$ P14 mice and stained with anti-Vβ8.1/8.2, anti-CD8a, and anti-CD45.1 mAbs. Vβ8.1/8.2$^+$CD8$^+$CD45.1$^+$ cells were then adoptively transferred into congenically distinct wild-type recipients before infection with either 1x10^5 plaque-forming units (PFU) of LCMV-Armstrong or 1x10^6 PFU LCMV-Clone 13. LCMV-Armstrong was injected intraperitoneally and LCMV-Clone 13 was injected intravenously. For Division 1 analyses, CD8$^+$ P14 T cells were first labeled with CFSE prior to transfer. 10mM CFSE was diluted 1:1000 in pre-warmed PBS. 40x10^6 cells were washed with pre-warmed PBS and resuspended in 500 µL PBS and 500 µL diluted CFSE. Cells were then placed in a thermomixer at 37° C, 1400 RPM, incubated for 9 minutes and quenched with 500 µL FBS. Cells then rested in culture medium (Isocove's modified Dulbecco's medium + 10% fetal bovine serum (v/v) + 2 mM glutamine + penicillin (100 U/mL) + streptomycin (100 µg/ml) + 55 mM β-mercaptoethanol) for 5 minutes and washed. To conduct the depletion experiments, congenically distinct naïve splenocytes from either *Ezh2*$^{fl/fl}$*Cd4*$^{Cre+}$ and *Ezh2*$^{fl/fl}$*Cd4*$^{Cre-}$ P14 mice; or *Ezh2*$^{fl/wt}$*Cd4*$^{Cre+}$ and *Ezh2*$^{fl/wt}$*Cd4*$^{Cre-}$ P14 mice; or *Ifnar1*$^{-/-}$ and *Ifnar1*$^{+/+}$ P14 mice were harvested, stained, and counted as above and adoptively transferred at a 1:1

ratio into congenically distinct hosts. These mice were then infected intravenously with $2x10^6$ PFU LCMV-Clone 13. For Division 1 analyses, $3x10^6$ cells were transferred; for Day 4 analyses, $1x10^6$ cells were transferred; for all other time point analyses, $1x10^4$ cells were transferred. For adoptive co-transfer experiments analyzed at days 5 or 7 post-infection, a total of $2x10^4$ cells were transferred.

10x Genomics library preparation and sequencing

P14 T cells ($CD8^+CD45.1^+$) were sorted from the spleen and resuspended in phosphate-buffered saline (PBS) + 0.04% (w/v) bovine serum albumin. About 10,000 cells per sample were loaded into Single Cell A chips or Single Cell G chips (10x Genomics) and partitioned into Gel Bead In-Emulsions in a Chromium Controller (10x Genomics). Single-Cell RNA libraries were prepared according to the 10x Genomics Chromium Single Cell 3' Reagent Kits v2 User Guide or Next GEM Single Cell 3' Reagent kits v3.1 User Guide and sequenced on a HiSeq 4000 (Illumina).

Ezh2 overexpression experiments

The MSCV-mouse-Ezh2-IRES-GFP (Ezh2 overexpression, Ezh2-OE) vector was purchased from Addgene (Cat # 107146). To generate retroviral particles, Platinum-E (Plat-E) cells were plated in 10 cm plates 1 day prior to transfection and transfected with 10 µg of the Ezh2-OE or empty vector and 5 µg of pCL-Eco using TransIT-LTI (Mirus). The supernatant was collected at 48 and 72 hours post-transfection and stored at -80°C. Spleens and lymph nodes were harvested from naïve $CD45.1^+$ and $CD45.1.2^+$ P14 mice and whole splenocytes were activated *in vitro* with LCMV $GP33_{33-41}$ peptide

for 1 hour at 37°C. $1x10^6$ activated splenocytes were plated in a 48-well plate and incubated for 36 hours at 37°C. P14 cells were transduced with empty vector (EV) or Ezh2 OE retroviruses. For transduction, retroviral supernatant was added to the plated cells, supplemented with polybrene (8 μg/mL, Millipore), and centrifuged for 90 minutes at 900 rcf at room temperature. Retroviral supernatant was replaced with culture medium (Isocove's modified Dulbecco's medium + 10% fetal bovine serum (v/v) + 2 mM glutamine + penicillin (100 U/mL) + streptomycin (100 μg/ml) + 55 mM β-mercaptoethanol), and cells were rested for 2 hours at 37°C . Cells were washed 3 times with PBS and counted. Based on a previous test of transduction efficiency, a 1:1 ratio of P14 cells transduced with EV and Ezh2-OE retroviruses (total of $2x10^4$ P14 cells) were adoptively transferred into a congenically distinct host. One hour later, recipient mice were infected with $2x10^6$ PFU of LCMV-Clone 13. Seven days later, spleens were harvested and analyzed by flow cytometry.

In vivo IFNAR1 blockade

Naive splenocytes were harvested and adoptively transferred and recipient mice infected with LCMV-Cl13 and as described above. Recipient mice were intraperitoneally injected with 500 μg of either Mouse IgG1 (MOPC-21) or anti-mouse IFNAR-1 (MAR1-5A3) mAb purchased from BioXCell on day of transfer and day of infection. On days 2 and 4 post-infection, recipient mice were injected with 250 μg of either antibody as previously described (EB et al. 2013). Mice were sacrificed at day 2 (for Division 1 analysis) or day 5 post-infection.

Single-cell RNA-seq data analysis

The single-cell RNA sequencing data were aligned and quantified using the Cell Ranger Single-Cell Software Suite against the GRCm38 (mm10) mouse reference genome. The preliminary filtered data generated from Cell Ranger were used for the downstream analysis. Further quality control was applied to cells based on two metrics, including the number of detected genes and proportion of mitochondrial gene count per cell. Specifically, cells with less than 200 detected genes were excluded, as well as cells with more than 30% mitochondrial gene count. Genes that were expressed in less than 3 cells in the dataset were also removed. After quality control, we normalized the sequencing depth for each cells by applying the *normalize_total* function in Scanpy (Wolf, Angerer and Theis 2018) to the raw counts. The logarithmized normalized count matrix was then used for the downstream analysis. The normalized and logarithmized single-cell data were processed for dimension reduction and unsupervised clustering following the workflow in Scanpy (Wolf et al. 2018). In brief, a principal component analysis (PCA) matrix was first calculated to reveal the main axes of variation and denoise the data by using *scanpy.tl.pca* function with default parameters. For visualization, the dimensionality of each dataset was further reduced using Uniform Manifold Approximation and Projection (UMAP) implemented in the *scanpy.tl.umap* function with default parameters. We used Leiden, an unsupervised graph-based clustering algorithm, to cluster single-cells by their expression profiles, with *sc.tl.leiden* function and default settings. The differentially expressed genes were identified by using the *scanpy.tl.rank_genes_groups* function with default parameters.

RNA velocity analysis

The aligned single-cell reads (in .bam files) from Cell Ranger software were first counted for spliced and unspliced mRNAs using the velocyto package (La Manno et al. 2018). The velocity estimation and visualization of the samples were then obtained with the scVelo package (V et al. 2020). We first computed the first- and second-order moments for velocity estimation using the *scvelo.pp.filter_and_normalize* and *scvelo.pp.moments* functions with default settings. RNA velocity was then estimated with the generalized dynamical model in scVelo using *scv.tl.recover_dynamics* and *scvelo.tl.velocity.* We used the *scv.tl.velocity_graph* function to project the velocities onto a lower-dimensional embedding (UMAP) by translating them into likely cell transitions and to calculate the probabilities of one cell transitioning into another cell. *scvelo.pl.velocity_embedding_stream* was used to visualize the velocities. The latent time status for each cell was also estimated from the velocities using the dynamical model with *scvelo.tl.latent_time* function while the driver genes for the dynamics were also predicted. The *scv.pl.scatter* function was used to visualize the latent time status and driver genes.

Single-cell ATAC-seq analysis

$CD8^+CD45.1^+$ P14 cells were CFSE labeled and adoptively transferred into $CD45.2^+$ recipients subsequently infected with LCMV-Armstrong or LCMV-Clone 13 as described above. At day 2 post-infection, mice were sacrificed and division 1 (2nd CFSE peak) of donor $CD8^+CD45.1^+$ P14 cells were FACS-isolated. Nuclei were then isolated, ~3,000 nuclei per sample were loaded into Next GEM H chips (10x Genomics) and partitioned into GEMs in a Chromium Controller (10x Genomics). ATAC libraries were sequenced

from both ends using an Illumina Hiseq. The Cellranger ATAC pipeline (1.2.0) (AT et al. 2019) was used to preprocess the sequencing data. Firstly, we started from fastq files and the reads were mapped to mm10 genome using cellranger-atac count program. Peaks were also identified within each sample individually. We next pooled the returned results from all samples to produce a single peak-barcode matrix using cellranger-atac aggr with option --normalize=signal. This enables the direct comparison between groups (i.e. LCMV-Arm vs LCMV-Clone13) in the downstream analysis. The returned aggregated files were loaded into Signac (1.5.0) (T et al. 2021), a R (4.0.2) (R core team, 2021) package, for downstream analysis using the standard Signac/Seurat pipeline. With Signac, QC metrics were first calculated for each cell which include the total number of fragments in peaks, fraction of all fragments that fall within ATAC-seq peaks, nucleosome signal strength, and the ratio of reads in genomic blacklist regions provided by ENCODE project (Consortium 2012). Outlier cells in the QC metric categories were removed per Signac's standard processing guidelines. Differentially accessible regions were identified by *FindMarkers* function and each peak was also annotated by its closest gene using *ClosestFeature*.

Latent semantic indexing (LSI), a form of dimensional reduction, was performed using Signac's '*RunTFIDF'* and '*RunSVD'* functions. LSI dimensions that were highly correlated with read depth were identified using Signac's 'DepthCor' and were not used in downstream analysis. The UMAP hyperparameters were varied to produce consistent object shapes (using R). Once hyperparameters were chosen, we ran Signac/Seurat's '*RunUMAP'* function on the LSI dimensions chosen earlier to compute the UMAP embedding. Signac/Seurat's '*FindNeighbors'* function was run using the same LSI

dimensions as UMAP to compute the nearest neighbors graph. Signac/Seurat's '*FindClusters'* was then run to identify the clusters of the cells with resolution set to 0.2. Additionally, the read density was visualized in Integrated Genome Browser (NH, DC and AE 2016) using the bigwig files generated in the *cellranger-atac* count step. The heatmap and density plots were generated using the same bigwig files and the bed files of differentially accessible peaks with the *computeMatrix* and *plotHeatmap* functions of DeepTools software.

H3K27me3 deposition analysis

$CD8^+CD45.1^+$ P14 cells were adoptively transferred into $CD45.2^+$ recipients subsequently infected with LCMV-Armstrong or LCMV-Clone 13 as described above. At day 7 post-infection, mice were sacrificed and donor $CD8^+CD45.1^+$ P14 cells were FACS-isolated, stained with anti-H3K4me3, anti-H3K27me3, or isotype IgG control mAbs (Cell Signaling), and processed for the CUT&RUN Assay Kit (Cell Signaling). CUT&RUN libraries were sequenced from both ends using an Illumina HiSeq 4000 to a total read length of 101 bp from each end. The reads were firstly trimmed with trimmomatic v0.36 to remove the sequencing adapters and then aligned against the mouse genome (GRCm38) using Bowtie2 (Langmead and Salzberg 2012) with parameters set as --local --very-sensitive-local --no-unal --no-mixed --no-discordant --phred33 -I 10 -X 700. Spike-in normalization is used for calibrating the epitope abundance between experiments as described (Zheng and Song 2020). In the Spike-in normalization, the trimmed reads were also aligned against yeast genome (sacCer3) with Bowtie2 with two more parameters --no-overlap and --no-dovetail, to avoid possible

cross-mapping of the experimental genome to that of the carry-over yeast DNA which is used for calibration. The genomic coverage was then normalized by applying the scaling factor that is calculated from the number of mapped reads to mouse genome and yeast genome (Zheng and Song 2020). MACS2 (Zhang et al. 2008) was used for peak calling analysis: (1) we first used the Callpeak program to obtain the peaks for each sample based on the spike-in normalized alignment files; (2) we next used the bdgcmp program to compare H3K4me3 or H3K27me3 samples against their corresponding IgG samples which generated the relative binding signals from read signals (i.e. the fold-enrichment of H3K4me3 or H3K27me3 against IgG samples) for each peak region found in (1). The returned BedGraph files in (2) were visualized in Integrated Genome Browser (NH et al. 2016). The heatmap and density plots were generated using the relative binding signals with the computeMatrix and plotHeatmap functions of DeepTools software. Motif analysis on the peak regions were implemented using findMotifsGenome.pl program in HOMER software.

Functional enrichment analysis

Pathway analyses were implemented with PANTHER using Fisher's exact test and the default settings (H et al. 2021) or Metascape (Zhou et al. 2019).

Supplementary Table 1: Division 1 scRNA-seq DE gene analysis indicating fold change, adjusted p-value and Z-score of the top 150 DE genes comparing the $Div1_{ARM\text{-}MEM}$ cluster over the $Div1_{CL13}$ & $Div1_{ARM\text{-}EFF}$ clusters

Gene name	Fold change	Adjusted p-value	Z-score
Tgtp1	23.52903586	4.16E-05	4.2341304
Cnrip1	21.41524088	0.866331805	0.18735689
Sfxn3	20.89532800	0.03080449	2.2805376
Junb	16.64666187	0	38.805367
Itgae	16.58874684	0.322238159	1.0719545
Tgtp2	15.78353332	1.79E-07	5.358969
Klf2	15.22105233	2.92E-188	29.438538
Gm43698	15.15265820	0.001852604	3.2451382
Tsc22d3	14.24968181	5.54E-50	15.065321
Ltb	13.25921078	8.19E-109	22.359304
Sell	12.64808445	4.16E-71	18.041683
Dusp1	12.26217080	3.30E-80	19.177006
Ifit3	11.70171110	8.99E-72	18.127287
Ifitm10	11.32560018	0.417750947	0.8813637
Btg1	11.15471385	1.90E-170	28.007277
Dnajb9	10.67165776	8.77E-08	5.488919
Hsd11b1	10.66703414	0.000226705	3.8213282
Aqp3	10.58174242	0.89509642	0.14745055
Tcp11l2	10.16446657	0.01027675	2.693826
Ppp1r15a	10.09177471	9.50E-72	18.123947
Rnaset2a	9.64529725	1.32E-28	11.259951
Hid1	9.56919789	0.467032572	0.7930963
Tmem71	9.55341145	0.0174304	2.5025165
Dusp10	9.49000272	4.64E-07	5.1787357
Tnfaip3	9.36156935	6.40E-46	14.421027
D930028M14Rik	9.24288799	0.911082589	0.12555279
Acss1	9.08773584	0.717071283	0.39745703
Ypel3	9.02507237	1.41E-17	8.68335
Irf7	8.79736213	1.29E-118	23.35005
Ddx60	8.76799758	0.031440361	2.2721884

Supplementary Table 1: Division 1 scRNA-seq DE gene analysis indicating fold change, adjusted p-value and Z-score of the top 150 DE genes comparing the $Div1_{ARM\text{-}MEM}$ cluster over the $Div1_{CL13}$ & $Div1_{ARM\text{-}EFF}$ clusters

Gene name	Fold change	Adjusted p-value	Z-score
Lcn4	8.56829053	0.061951602	1.9811554
Cd7	8.54569010	3.72E-05	4.259558
Tnfrsf25	8.47330793	0.798744919	0.2821133
Fam89b	8.33698477	0.740709486	0.3629617
Rnaset2b	8.33310986	2.25E-20	9.403502
Cd55	8.32450911	0.282462891	1.1611308
Maff	8.27856951	0.058585357	2.0074918
Lrrc8a	7.93609227	0.281435253	1.163625
Ifit1	7.82684568	1.02E-42	13.891085
Dapl1	7.81127093	2.31E-30	11.619741
Ramp1	7.67925737	0.094839442	1.7790662
Vps37b	7.64980514	9.83E-39	13.198895
Pydc3	7.52488587	4.93E-14	7.6790752
Ifit3b	7.40302397	5.56E-11	6.696677
Hbp1	7.27648951	0.194878122	1.3930019
Shisa5	7.22782512	6.02E-281	35.98975
Dzip1	7.18139790	0.673503769	0.46183982
Armc3	7.17337375	0.647784314	0.5009007
Gm8797	7.14213152	2.25E-05	4.374627
Tmem108	7.01397651	0.068158563	1.9365356
Evl	6.94434585	4.52E-32	11.958544
Trim13	6.90659487	0.578164164	0.608149
Ifi206	6.85152483	1.77E-27	11.023514
4930481A15Rik	6.67778942	0.982358725	-0.024328496
Ifi209	6.65950386	3.29E-28	11.17701
Ifi203	6.54314844	3.64E-34	12.362046
Trim14	6.53921066	0.641077891	0.511152
Sh3bp5	6.40277361	0.339220684	1.0365081
Tob1	6.39266282	0.079996766	1.8615421
Rps27rt	6.31513992	3.12E-273	35.486504
Actn2	6.30450893	0.54045445	0.66739553
Ifi214	6.26099349	4.42E-08	5.612189
4930570N18Rik	6.23494918	0.717186552	0.3972034

Supplementary Table 1: Division 1 scRNA-seq DE gene analysis indicating fold change, adjusted p-value and Z-score of the top 150 DE genes comparing the $Div1_{ARM\text{-}MEM}$ cluster over the $Div1_{CL13}$ & $Div1_{ARM\text{-}EFF}$ clusters

Gene name	Fold change	Adjusted p-value	Z-score
Baiap3	6.18014505	0.691306694	0.43548217
Gbp8	6.17681362	0.009210631	2.7321682
Gm45837	6.16489405	0.073962525	1.8987006
Gm8953	6.10572452	0.44875342	0.82475924
Ifi213	6.09421754	1.66E-11	6.875178
Grcc10	6.02912358	0.000465374	3.633485
Jund	6.00975218	2.12E-231	32.651505
Nsg2	5.94831645	0.05739855	2.017067
Pacsin1	5.90840778	0.443604596	0.8342286
Tnfrsf26	5.81463003	0.658646535	0.4842026
Pnrc1	5.80254457	5.66E-32	11.939225
Rps18-ps3	5.77589213	5.01E-36	12.709536
Rpl13-ps3	5.76243511	1.49E-38	13.166388
Frat2	5.72482939	0.010057842	2.7014565
Gm28935	5.65229514	0.604933796	0.5657485
Ikbke	5.63571752	0.091335254	1.7976243
Rarg	5.62947740	0.93574567	0.090338826
Cd69	5.57934359	2.23E-65	17.288366
Pecam1	5.57235704	0.283180718	1.1593765
Rab4b	5.53145225	0.592407358	0.58557487
Tdrp	5.50863434	0.385977587	0.94255483
Epsti1	5.46890234	1.12E-36	12.828706
Cxcr4	5.40913161	0.228903208	1.2962164
Nme3	5.40308995	0.980257043	0.028281083
Ciart	5.38090188	0.550744393	0.65116245
Malat1	5.31636258	2.47E-221	31.927864
Ubb	5.30499172	0	40.190845
Arl4c	5.28341817	8.65E-15	7.9044785
Oasl2	5.28249611	2.40E-09	6.1094327
Pik3ip1	5.27618445	0.002136878	3.2020612
Ulk3	5.27218867	0.807873768	0.2695369
Gm42726	5.25634037	0.949749558	0.07135795
Gm9844	5.25166394	1.06E-08	5.8610115

Supplementary Table 1: Division 1 scRNA-seq DE gene analysis indicating fold change, adjusted p-value and Z-score of the top 150 DE genes comparing the $Div1_{ARM\text{-}MEM}$ cluster over the $Div1_{CL13}$ & $Div1_{ARM\text{-}EFF}$ clusters

Gene name	Fold change	Adjusted p-value	Z-score
Rab37	5.24950431	0.29551205	1.1315815
Reck	5.23775363	0.880344727	0.16803783
Phf11c	5.20664195	4.24E-05	4.2295437
Il6ra	5.18142887	0.515180399	0.7109163
Serpini1	5.18133441	0.754864874	0.3428817
Gm8730	5.15392520	6.16E-176	28.457111
Mcoln2	5.13634924	0.981162278	0.025956033
Ifit1bl1	5.11682680	1.34E-05	4.489696
Lef1	5.08597792	1.29E-05	4.4984045
Dnaja4	5.06351561	0.522431293	0.6990162
Zfp36l2	5.05949467	6.27E-21	9.5401945
Ripor2	5.05144591	0.186551845	1.4189368
Rtp4	5.04950441	2.42E-27	10.994726
Jakmip1	5.04650296	0.467758479	0.7917858
G430095P16Rik	5.04127061	0.91031643	0.12663077
Ube2l6	5.03955029	0.002103616	3.2070496
Rapgef4	5.01791628	0.649591499	0.49806836
Gab3	4.98443610	0.657645025	0.48574558
Gm2000	4.97444509	1.98E-109	22.422905
Selenop	4.94106625	0.289421231	1.1451937
Gm6133	4.93346851	4.35E-16	8.276761
Itgb7	4.90942819	3.80E-07	5.217036
Smpd5	4.90129268	0.980257043	0.028281083
Klrd1	4.89410075	2.01E-06	4.8896894
Rnf166	4.86141602	0.061643871	1.9835017
Tmsb10	4.84761324	5.78E-300	37.19586
Cyth1	4.83347674	0.108428386	1.7123371
Izumo4	4.75927395	0.846579599	0.21631436
Fbxo32	4.75805583	0.87130097	0.1801915
Gramd1a	4.75106650	0.002313356	3.1780286
S1pr1	4.72836039	0.67187519	0.46460876
Gbp9	4.72816244	0.000260888	3.7850785
Herc3	4.71955488	0.750800774	0.34875774

Supplementary Table 1: Division 1 scRNA-seq DE gene analysis indicating fold change, adjusted p-value and Z-score of the top 150 DE genes comparing the $Div1_{ARM\text{-}MEM}$ cluster over the $Div1_{CL13}$ & $Div1_{ARM\text{-}EFF}$ clusters

Gene name	Fold change	Adjusted p-value	Z-score
Cd200r4	4.68580852	0.981131225	0.026907189
Irgm1	4.68397410	4.71E-09	5.9977036
Klf3	4.67951496	0.065514453	1.9551994
Cd3g	4.66886314	1.97E-107	22.21642
Socs1	4.62323597	0.000814378	3.4809828
Gm19705	4.58031462	0.092512952	1.7915369
Ms4a4c	4.55936529	2.29E-25	10.567275
Gbp6	4.55007397	0.377759819	0.95851314
Ccng2	4.53512212	0.515887884	0.7092887
Phf11d	4.53448498	0.322238159	1.07187
Mndal	4.52390740	2.69E-24	10.328281
Parp8	4.51602102	0.836729851	0.22984193
Ggt1	4.50576415	0.808052952	0.26919872
Cyp4v3	4.50442608	0.86276898	0.19272564
Cd3e	4.49383701	2.05E-49	14.977138
Gm17541	4.43918921	0.6653481	0.474226
Tm6sf1	4.40718360	0.189158956	1.411095
Clec2i	4.40281523	0.677826494	0.4555833
Gm12166	4.39076159	0.754127868	0.34414992
2610035D17Rik	4.38253496	0.990911893	-0.012090269
Il2rg	4.37723852	7.59E-35	12.490664

Supplementary Table 2: Division 1 scRNA-seq DE gene analysis indicating fold change, adjusted p-value and Z-score of the top 150 DE genes comparing the $Div1_{CL13}$ cluster over the $Div1_{ARM\text{-}EFF}$ & $Div1_{ARM\text{-}MEM}$ clusters

Gene name	Fold Change	Adjusted p-value	Z-score
Hist1h2ap	35.3324283	1.13E-247	33.862354
Il21	33.78767093	3.94E-17	8.489918
Gpr55	28.90240218	0.236302881	1.2239625
Lancl3	28.65379656	0.325969221	1.0159382
Slc15a3	25.28034943	0.000182714	3.8099518

Supplementary Table 2: Division 1 scRNA-seq DE gene analysis indicating fold change, adjusted p-value and Z-score of the top 150 DE genes comparing the $Div1_{CL13}$ cluster over the $Div1_{ARM\text{-}EFF}$ & $Div1_{ARM\text{-}MEM}$ clusters

Gene name	Fold Change	Adjusted p-value	Z-score
Hist1h2ap	35.3324283	1.13E-247	33.862354
Hist1h2ab	22.75327484	0.000419246	3.5943267
AY036118	21.5771737	8.40E-271	35.41841
Tyrobp	20.8153657	0.007613577	2.728782
Dancr	19.10126923	2.60E-10	6.3952284
Tirap	16.76065471	0.023511769	2.3217156
Hist1h3c	16.45745559	1.01E-29	11.401396
Zpbp2	16.18151745	3.84E-06	4.690935
Hist1h4b	16.10525948	2.55E-12	7.0761986
Tigit	15.24492344	0.003349463	2.9959056
Hist1h3a	14.31898971	6.04E-09	5.8894615
Fcer1g	14.03900223	0.075389353	1.8289479
Gm42418	12.67551624	2.19E-246	33.762768
Cacna1s	12.668838	0.00249506	3.0862927
Hist2h4	12.47936222	0.00068774	3.4604518
Hist1h2bb	12.15081012	0.005501774	2.837199
Il10	12.01396616	9.20E-113	22.706358
Hexim2	11.83667935	0.010135255	2.6303837
H2-Eb1	11.69637365	0.049756155	2.0147102
Espl1	11.34919134	2.86E-32	11.904766
E330009J07Rik	11.11591498	0.000298741	3.6838286
Gm20628	10.7975291	1.48E-32	11.959957
Smarcal1	10.75448101	1.79E-07	5.292444
Gm28727	10.68899715	3.74E-06	4.696247
Ell2	10.67783533	0.000755017	3.4344757
Ctla4	10.59791532	3.44E-119	23.365025
Gm26917	10.57691875	3.79E-209	31.095093
Hist1h3e	10.44389896	5.09E-10	6.2907844
Cdkn2a	10.39909446	0.798832849	0.26736125
Tnfrsf4	10.12537124	1.67E-119	23.396915
Gm26847	9.706971795	0.00012022	3.9146118
Fcgr2b	9.698203994	0.624327511	0.5112728
Pla1a	9.641963711	0.043468428	2.0723195

Supplementary Table 2: Division 1 scRNA-seq DE gene analysis indicating fold change, adjusted p-value and Z-score of the top 150 DE genes comparing the $Div1_{CL13}$ cluster over the $Div1_{ARM\text{-}EFF}$ & $Div1_{ARM\text{-}MEM}$ clusters

Gene name	Fold Change	Adjusted p-value	Z-score
H2-Aa	9.602741223	0.087777752	1.7567633
Tlcd2	9.533619192	0.026151164	2.2801497
Tmem154	9.408655004	0.050749746	2.006181
Fancb	9.233910826	0.003839731	2.9527633
Hist1h3i	9.18037827	0.01375752	2.5222259
Zfp316	9.159674301	1.94E-16	8.301284
Cox6b2	9.134012094	0.269961356	1.140701
BC028528	9.114775357	9.60E-06	4.4964495
Hk2	9.011685715	4.60E-182	29.004074
Abcb1b	8.956510123	2.77E-96	20.936316
Med12l	8.875471111	0.737571725	0.35053647
Hist1h2ai	8.710973759	0.000248494	3.7316997
Gm10184	8.642148372	0.000129309	3.896582
Maf	8.580212629	3.02E-18	8.786732
Loxl2	8.423676309	1.13E-149	26.270391
Pgk1	8.421166563	5.68E-139	25.290232
Ptprk	8.385735931	1.29E-15	8.07063
Lars2	8.34079789	1.98E-70	17.834736
Pak6	8.303863335	0.141747087	1.5149463
Ptger2	8.245791602	0.061373776	1.9227467
Gfod1	8.229324428	0.004045567	2.936245
Gm26737	8.191365676	4.23E-73	18.178406
Sh3rf1	8.142630858	0.000779509	3.4255579
Pou2af1	7.829390492	2.97E-10	6.3743696
Fgl2	7.75606987	0.340710718	0.9856652
Gm9828	7.7462953	0.000172691	3.8242893
Bcl2a1d	7.744542414	9.12E-118	23.220913
1810009A15Rik	7.74105393	2.22E-26	10.705743
Wfikkn2	7.718483929	0.269961356	1.1406578
Ifng	7.684500573	1.55E-150	26.34793
Rab11fip4	7.647465005	2.41E-08	5.6531725
H2-Ab1	7.509844316	0.035442332	2.157611
Slc22a15	7.382780675	0.591968011	0.5585177

Supplementary Table 2: Division 1 scRNA-seq DE gene analysis indicating fold change, adjusted p-value and Z-score of the top 150 DE genes comparing the $Div1_{CL13}$ cluster over the $Div1_{ARM\text{-}EFF}$ & $Div1_{ARM\text{-}MEM}$ clusters

Gene name	Fold Change	Adjusted p-value	Z-score
Rab26os	7.373738224	2.87E-89	20.139544
Hist1h2bg	7.373238888	0.005106837	2.861426
2810429I04Rik	7.366704637	0.191540853	1.3485959
Snrnp35	7.276238337	1.62E-17	8.593865
Napsa	7.244964898	0.624507668	0.5108841
Pdcd1	7.244691716	5.03E-75	18.42236
Zfp219	7.227748969	1.75E-22	9.833288
1700047I17Rik2	7.026803719	0.037841465	2.1305552
2010015M23Rik	6.764709588	1.78E-05	4.3613653
Tfdp1	6.745091434	0.00010887	3.9389467
C1qtnf12	6.730424961	0.000128156	3.8987842
Metrnl	6.706862848	0.405553603	0.86092395
Naaa	6.656805427	0.267680178	1.1460345
St14	6.647385398	0.325969221	1.015895
Aunip	6.642210756	7.99E-40	13.287436
Atp2b4	6.62339225	6.70E-11	6.601763
Alcam	6.570006054	1.24E-17	8.624829
Rpl7a-ps3	6.540212448	0.042619513	2.0808918
Cetn4	6.534363443	9.13E-22	9.663569
Arl15	6.520858888	0.392751918	0.88443846
Dcxr	6.516390224	0.340835377	0.9852765
Gm5611	6.503933471	4.84E-22	9.729103
Mcm10	6.498529504	3.31E-81	19.185902
Hes1	6.484582088	1.86E-18	8.841534
Eid2	6.476160317	3.77E-10	6.3376837
Dqx1	6.463721327	6.33E-64	16.967875
Cmss1	6.462014554	2.56E-53	15.45513
Cela1	6.457317658	0.097049991	1.7081581
Slc8b1	6.448302837	0.22313756	1.2583814
Hpdl	6.43928007	0.000108957	3.9386876
Gm30211	6.435303544	0.848014176	0.20197845
Eif2ak4	6.433173954	3.26E-05	4.2247267
Gzmb	6.428166065	7.01E-112	22.615389

Supplementary Table 2: Division 1 scRNA-seq DE gene analysis indicating fold change, adjusted p-value and Z-score of the top 150 DE genes comparing the $Div1_{CL13}$ cluster over the $Div1_{ARM\text{-}EFF}$ & $Div1_{ARM\text{-}MEM}$ clusters

Gene name	Fold Change	Adjusted p-value	Z-score
Aarsd1	6.401198291	0.021568421	2.3550117
8030462N17Rik	6.400622398	1.16E-09	6.1595006
Fes	6.398871966	0.080465275	1.7983294
Pidd1	6.391159977	2.71E-25	10.469432
Farp1	6.342351344	0.077644211	1.8151717
Gm17275	6.320372552	0.214350522	1.2825652
Entpd1	6.319060156	0.370797668	0.9261124
Runx2os1	6.300081535	6.33E-07	5.052419
Epb41l4aos	6.265800345	6.05E-165	27.600805
Aldh7a1	6.249073895	1.50E-15	8.052104
Lag3	6.247511708	3.24E-129	24.35926
Plagl2	6.238120409	1.20E-43	13.935217
E2f8	6.214636461	6.31E-26	10.607626
Cpd	6.204055533	8.49E-06	4.5230517
Myl6b	6.201125984	0.061356657	1.9229194
Car12	6.193823619	7.92E-33	12.012017
Cenph	6.18205633	4.79E-101	21.463697
Fbxw8	6.178351708	1.84E-33	12.132915
Wee1	6.177576195	2.51E-27	10.906944
Hist1h2bj	6.172513129	3.28E-66	17.277514
Hells	6.152424293	5.13E-161	27.267479
Fam72a	6.127050321	6.26E-22	9.702544
Rdh10	6.120358664	0.00286444	3.044187
Mnd1	6.102491582	1.64E-15	8.041135
Hist1h2ak	6.093818369	1.47E-23	10.081388
Mfsd13a	6.071838003	0.004494666	2.9027114
Ccr2	6.042790812	0.280027634	1.1166683
Gm26518	6.040225036	3.64E-17	8.49944
Furin	6.038937743	2.61E-117	23.17449
Tppp3	6.028499674	0.653165291	0.46921015
Calcrl	6.016110226	0.118668072	1.607644
Tm9sf1	5.98093484	0.000273697	3.7067385
1110002L01Rik	5.978377509	6.39E-08	5.4803658

Supplementary Table 2: Division 1 scRNA-seq DE gene analysis indicating fold change, adjusted p-value and Z-score of the top 150 DE genes comparing the $Div1_{CL13}$ cluster over the $Div1_{ARM\text{-}EFF}$ & $Div1_{ARM\text{-}MEM}$ clusters

Gene name	Fold Change	Adjusted p-value	Z-score
Eea1	5.971445479	9.90E-50	14.909503
Hmga1	5.965605183	4.92E-120	23.449753
Cenpi	5.960381191	5.49E-07	5.0800366
Zfp866	5.943663747	0.162232957	1.4417685
2700038G22Rik	5.93682711	6.91E-70	17.76389
Nt5dc3	5.888226631	0.001324612	3.2752292
Serpinb6b	5.885279776	1.20E-134	24.881374
Stk11ip	5.87690998	0.001442155	3.2504191
Snhg9	5.876312012	2.93E-153	26.588171
Ccr5	5.871967568	0.002285645	3.113111
Hist1h2ae	5.764593191	5.04E-52	15.260709
Naif1	5.751424405	0.05906596	1.9400425
Ptcra	5.738173937	3.05E-10	6.3704615

Supplementary Table 3: Division 1 scRNA-seq DE gene analysis indicating fold change, adjusted p-value and Z-score of the top 100 DE genes comparing the $Div1_{ARM\text{-}EFF}$ cluster over the $Div1_{ARM\text{-}MEM}$ & $Div1_{CL13}$ clusters.

Gene name	Fold Change	Adjusted p-value	Z-score
Mt3	27.75308032	0.001729264	3.270873
2210011C24Rik	13.10623409	0.990703368	0.012229
Nccrp1	11.69157511	0.966609314	0.044686
Car5b	7.940533275	0.93861291	0.082136
Eif2s3y	7.058313452	0.361868954	0.979468
Ctla2a	7.04843371	1.09E-20	9.5256
Rab39b	6.724858445	0.969497671	0.040813
1500009L16Rik	6.3546823	0.797422428	0.272904
Ddx3y	5.454201877	0.529679025	0.673853
Ctla2b	5.438873608	0.576428832	0.596659
Gdpd5	5.105142034	0.890404177	0.146744
Gzmk	5.000616957	0.524668326	0.682107
Dkkl1	4.621556434	0.987269888	0.017528

Supplementary Table 3: Division 1 scRNA-seq DE gene analysis indicating fold change, adjusted p-value and Z-score of the top 100 DE genes comparing the $Div1_{ARM-EFF}$ cluster over the $Div1_{ARM-MEM}$ & $Div1_{CL13}$ clusters.

Gene name	Fold Change	Adjusted p-value	Z-score
Tspan2	4.535201338	0.969883254	-0.040202
Gpr160	4.167753926	0.993583777	0.008407
Gm15518	4.078412499	0.89733476	-0.13742
Dusp14	4.047645663	0.946148962	-0.0722
Grb7	3.887095627	0.993583777	0.008305
Myl4	3.563350259	0.7816802	-0.295502
Gzmb	3.355073332	1.92E-37	13.06497
Lgals1	3.31577658	1.91E-31	11.9277
Hmgb2	3.197166549	1.37E-68	17.79315
Aplp1	3.118622653	0.912082605	-0.117599
Zdhhc2	3.116291089	0.827902245	-0.23046
Endod1	3.10873211	0.996121335	0.004993
Mt2	3.062693084	0.808824602	0.256446
Actg1	2.86028955	5.52E-108	22.36426
A430046D13Rik	2.764515384	0.906727496	-0.124682
Tmem163	2.761862124	0.492723129	-0.735735
H2afz	2.754283949	3.28E-75	18.64098
Ran	2.75116163	3.11E-59	16.51632
Gm9008	2.713873359	0.962746225	-0.050673
Uty	2.692830272	0.990703368	0.012229
E2f7	2.681406969	0.8061598	-0.260064
Klrk1	2.489692902	0.080959529	-1.856343
Ltb4r1	2.458723324	0.990703368	0.012229
Adap1	2.439669635	0.043016291	-2.143284
Tg	2.417720547	0.005224307	-2.924571
Gapdh	2.382398581	4.19E-34	12.44778
Hsp90aa1	2.381776268	5.07E-45	14.36287
4930486L24Rik	2.381461623	0.420493864	-0.865206
Pclaf	2.379214591	2.47E-18	8.917222
Tuba1b	2.362924609	5.12E-54	15.75949
Asns	2.36141319	0.349974626	-1.004333
Ncl	2.351598072	1.58E-34	12.52874
Esm1	2.349976126	0.860990784	-0.186029

Supplementary Table 3: Division 1 scRNA-seq DE gene analysis indicating fold change, adjusted p-value and Z-score of the top 100 DE genes comparing the $Div1_{ARM-EFF}$ cluster over the $Div1_{ARM-MEM}$ & $Div1_{CL13}$ clusters.

Gene name	Fold Change	Adjusted p-value	Z-score
Rapsn	2.339576171	0.405084701	-0.894784
Rps12	2.306508965	3.48E-41	13.72463
Prr5	2.293762468	0.688504824	-0.425763
Npm1	2.267537799	5.54E-66	17.4407
Lsr	2.241645586	0.846397091	-0.205519
Rps20	2.236113937	2.84E-63	17.07639
Havcr2	2.227041589	0.396644597	-0.911803
Arsb	2.222500125	0.472122692	-0.770867
Itgax	2.210271661	0.918572115	-0.108606
Rack1	2.197323522	5.10E-49	15.00253
Adam19	2.193657207	0.003843574	-3.025534
Rpl7a	2.187938066	1.41E-52	15.54284
Gen1	2.167267001	0.715544082	-0.386325
Mt1	2.125151952	0.60371565	0.552967
4930402H24Rik	2.109517418	0.918572115	-0.108606
Rps17	2.088278605	6.27E-47	14.67083
Rps27l	2.079489211	2.04E-27	11.09322
Kdelc2	2.079031331	0.6175979	-0.531643
Dut	2.047269033	2.52E-28	11.28671
Gm37387	2.043629689	0.909254885	-0.121268
Accs	2.042156881	0.8061598	-0.259962
Rps8	2.030509532	1.15E-69	17.93584
Bsn	2.010068546	0.257559289	-1.214769
Nrgn	1.969897741	0.990703368	0.012178
Rpsa	1.9632828	3.01E-59	16.51907
Hsp90ab1	1.962338057	3.18E-42	13.9019
Snai3	1.926390123	0.257309662	-1.215482
Rom1	1.905308048	0.290421394	-1.13513
Rpl28	1.899736953	6.47E-29	11.41111
F2rl3	1.891710472	0.27049346	-1.18277
Fhl2	1.877581198	0.040987744	-2.16448
Anp32b	1.876469967	1.81E-29	11.52848
Birc5	1.861274837	0.057947048	2.012208

Supplementary Table 3: Division 1 scRNA-seq DE gene analysis indicating fold change, adjusted p-value and Z-score of the top 100 DE genes comparing the $Div1_{ARM-EFF}$ cluster over the $Div1_{ARM-MEM}$ & $Div1_{CL13}$ clusters.

Gene name	Fold Change	Adjusted p-value	Z-score
Gzma	1.860351637	0.32289357	1.062318
2310031A07Rik	1.856908117	0.563750838	-0.616887
Cobll1	1.856620985	0.534243013	-0.66514
Prss30	1.856127996	0.936311811	-0.085142
Igfbp6	1.837902456	0.813128639	-0.250841
Zhx3	1.836082902	0.725195896	-0.373103
Rps2	1.812383975	5.92E-61	16.75722
Rps10	1.810339529	8.70E-36	12.76096
Rplp1	1.809860159	7.00E-84	19.68918
Rps21	1.804649171	6.20E-25	10.54145
Hint1	1.793726959	1.94E-29	11.52176
Rpl7	1.791028221	9.49E-42	13.82198
Anxa2	1.789944878	0.85556764	-0.193112
Gstt1	1.788757319	0.801657235	-0.267044
Rpl8	1.78704066	2.16E-76	18.78841
Hspe1	1.765930334	8.55E-16	8.215549
Lrrk1	1.758407043	0.89733476	-0.137318
Ska1	1.757825913	0.00022554	-3.828094
Bspry	1.757304745	0.011252034	-2.663361
Mmaa	1.756366521	0.578314515	-0.59378
Tubb4b	1.7503627	0.000207956	3.848985
Lamc1	1.749862909	0.51693276	-0.695533
Rps27a	1.742647811	2.04E-67	17.6344
Fam69b	1.739346061	0.388715955	-0.927292
Dhcr24	1.729999475	0.047690067	-2.098114
Epcam	1.7262261	0.778906924	-0.299501
Hmga1b	1.725207819	0.240423649	-1.258537
Klrg1	1.716868567	0.919998299	0.106695
E2f2	1.716687286	0.02358462	-2.387629
2010300C02Rik	1.712680272	0.882544243	-0.156986
Tmem2	1.701107955	0.608385816	-0.545247
Sapcd2	1.698818	0.014813807	-2.564436
Fut7	1.682869144	0.752697327	-0.335092

Supplementary Table 3: Division 1 scRNA-seq DE gene analysis indicating fold change, adjusted p-value and Z-score of the top 100 DE genes comparing the $Div1_{ARM-EFF}$ cluster over the $Div1_{ARM-MEM}$ & $Div1_{CL13}$ clusters.

Gene name	Fold Change	Adjusted p-value	Z-score
Rpl23	1.670124369	1.93E-43	14.10428
Rpl26	1.670070725	5.76E-57	16.19078
Cep72	1.668596934	0.671187735	-0.450984
Cacna1a	1.655432286	0.227121908	-1.294408
Phgdh	1.655286497	6.88E-06	4.643315
Rpl10a	1.654426879	8.31E-36	12.76481
Gm5141	1.652777879	0.729542979	-0.367294
Tpi1	1.644052762	3.13E-07	5.266062
Rpl30	1.633332033	2.80E-20	9.421044
Hopxos	1.632194516	0.982083342	-0.024152
S100a6	1.629637789	0.016243861	-2.530221
Txn1	1.619675118	1.00E-22	10.02609
Brca2	1.616614284	0.025842598	-2.351758
Nme1	1.608215645	2.25E-19	9.189514
Nebl	1.605685227	0.147357169	-1.549784
Plk1	1.602882009	4.29E-06	-4.743311
Ly6a	1.602389464	5.85E-22	9.840566
Rrm2	1.600156886	0.213211618	1.332445
Mif	1.596816397	1.26E-09	6.225964
Pcyox1l	1.594109023	0.527891575	-0.677215
Wdr31	1.593803256	0.400965212	-0.903141
Ldha	1.593773042	2.16E-23	10.18366
Rpl14	1.590929273	1.06E-57	16.29709
Serbp1	1.588539099	5.45E-18	8.824513
Vim	1.582183465	0.102738377	-1.738361
Zdhhc9	1.578848016	0.593684613	-0.568533
1700066M21Rik	1.57462654	0.565036766	-0.614849
Cdc25c	1.574051889	0.227687038	-1.292931
Rpl18	1.57248494	1.88E-35	12.69979
BC035044	1.565283904	0.036458044	-2.213013
Eef1b2	1.56231911	3.45E-18	8.877937
Ube2c	1.561701038	0.000927008	-3.450456
Slc25a23	1.558873435	0.619245258	-0.52907

Supplementary Table 3: Division 1 scRNA-seq DE gene analysis indicating fold change, adjusted p-value and Z-score of the top 100 DE genes comparing the $Div1_{ARM-EFF}$ cluster over the $Div1_{ARM-MEM}$ & $Div1_{CL13}$ clusters.

Gene name	Fold Change	Adjusted p-value	Z-score
Epas1	1.557811853	0.767006712	-0.315704
Atp5s	1.557057476	0.486290723	-0.746104
Soat2	1.549480823	0.527969343	-0.677012
Fbxo44	1.543720428	0.894558811	-0.141165
Pde4dip	1.542167639	0.397918143	-0.90872

Supplementary Table 4: Division 1 scATAC-seq DE gene analysis indicating differential areas of open chromatin between LCMV-Arm and LCMV-Cl13

LCMV-Armstrong	LCMV-Clone 13
Npm1	Akap9
Pcbp2	Tnfrsf9
Ybx1	Cops6
Cacybp	Lman1
Rpl38	Surf2
Snrpf	Nop58
Nap1l1	Rras2
Eif3j1	Mat2a
Lyar	Mtdh
Kpnb1	Pim3
Nfkbib	Pfdn2
Eif4e	Ahsa1
Nop58	Pcgf5
Srsf2	Mrps31
Bola2	Fkbp3
Rpl13a	Ssbp1
Rps21	Eif6
Bag3	Nolc1
Hspe1	Srsf7
Coro1a	Ddx39
Ly6e	Snrpa1
Rps25	Txn1
St3gal6	Pa2g4

Supplementary Table 4: Division 1 scATAC-seq DE gene analysis indicating differential areas of open chromatin between LCMV-Arm and LCMV-Cl13

LCMV-Armstrong	LCMV-Clone 13
Rpl3	Atp6v1f
Lck	Nfkbia
Rtp4	Rpl39l
Gramd3	Srsf2
Gm2682	Isg20
Malat1	H2-K1
Skap1	Ifi209
Epsti1	Skap1
Myo1e	Psma2
Fmnl2	Mndal
Pax3	Gimap9
Epha3	Serpinb9
App	Map4k1
Lgals3	Cxcl10
Atf3	Rrm2
Cdkn1a	Rnf213
Anxa2	Smchd1
Vim	Tuba1c
Myo5a	Batf3
Syt4	Cenpf
Higd1a	Prpf4b
Acsl3	Rab20
Ero1l	Snhg6
Fn1	Cdk1
Gpnmb	Thy1
Fmn1	Tnfrsf4
Dstn	Taf1d
Syne2	Hells
Pde11a	Ptpn22
Dct	Nkg7
Tyr	Pim1
Nrcam	Tnfsf8
Csrp1	Pla2g12a
Eps8	Lig1

Supplementary Table 4: Division 1 scATAC-seq DE gene analysis indicating differential areas of open chromatin between LCMV-Arm and LCMV-Cl13

LCMV-Armstrong	LCMV-Clone 13
Dst	Cd5
Atp1a1	Slamf7
Vcl	Cfl1
Litaf	Pfn1
Pde10a	Actb
Stox2	Lgals1
Mxi1	Myl6
Syngr1	Sh3kbp1
Fermt2	Serinc3
Rhoj	Plekha2
Nedd4l	Pclaf
Zeb2	Birc5
Zfand5	Cd47
Tom1l2	Slc16a10
Gpr137b	Rbbp6
Lmna	Tmem163
Chchd10	Crem
Lima1	Serpinb6b
Cpe	Zbtb32
Fam162a	Knl1
Tyrp1	Cnot6l
Cyb5a	Ccdc50
Ugp2	Traf1
Myo10	Snx5
Pmel	Car12
Met	Dek
Cd44	Ugcg
Mpzl1	Hsp90ab1
Nckap1	Brd2
Rab38	Rangap1
Ppfibp1	Slc38a1
5031439G07Rik	Mki67
Mitf	Gm26917
Meis2	Farp1

Supplementary Table 4: Division 1 scATAC-seq DE gene analysis indicating differential areas of open chromatin between LCMV-Arm and LCMV-Cl13

LCMV-Armstrong	LCMV-Clone 13
Sorbs1	Calm2
Ppargc1a	Ipo5
Ppp1r9a	Klf10
Plod2	Il2ra
Pgm2	AU020206
Tpm1	Rad21
H2-Aa	Furin
H2-Eb1	Malat1
Ctss	Hk2

REFERENCES

Abdel-Hakeem, M. S., S. Manne, J.-C. Beltra, E. Stelekati, Z. Chen, K. Nzingha, M.-A. Ali, J. L. Johnson, J. R. Giles, D. Mathew, A. R. Greenplate, G. Vahedi & E. J. Wherry (2021) Epigenetic scarring of exhausted T cells hinders memory differentiation upon eliminating chronic antigenic stimulation. *Nature Immunology,* 22**,** 1008-1019.

Alfei, F., K. Kanev, M. Hofmann, M. Wu, H. E. Ghoneim, P. Roelli, D. T. Utzschneider, M. von Hoesslin, J. G. Cullen, Y. Fan, V. Eisenberg, D. Wohlleber, K. Steiger, D. Merkler, M. Delorenzi, P. A. Knolle, C. J. Cohen, R. Thimme, B. Youngblood & D. Zehn (2019) TOX reinforces the phenotype and longevity of exhausted T cells in chronic viral infection. *Nature,* 571**,** 265-269.

Angelosanto, J. M., S. D. Blackburn, A. Crawford & E. J. Wherry (2012) Progressive Loss of Memory T Cell Potential and Commitment to Exhaustion during Chronic Viral Infection. *Journal of Virology,* 86**,** 8161-8170.

Aranda, S., G. Mas & L. D. Croce (2015) Regulation of gene transcription by Polycomb proteins.

AT, S., G. JM, Y. KE, Q. Y, M. F, M. GP, O. BN, M. MR, P. SE, C. MR, S. P, B. JC, J. D, N. CM, W. J, W. L, Y. Y, G. PG, C. ALS, Z. GXY, G. WJ & C. HY (2019) Massively parallel single-cell chromatin landscapes of human immune cell development and intratumoral T cell exhaustion. *Nature biotechnology,* 37.

Ataide, M. A., K. Komander, K. Knöpper, A. E. Peters, H. Wu, S. Eickhoff, T. Gogishvili, J. Weber, A. Grafen, A. Kallies, N. Garbi, H. Einsele, M. Hudecek, G. Gasteiger, M. Hölzel, M. Vaeth & W. Kastenmüller (2020) BATF3 programs CD8+ T cell memory. *Nature Immunology,* 21**,** 1397-1407.

Beltra, J.-C., S. Manne, M. S. Abdel-Hakeem, M. Kurachi, J. R. Giles, Z. Chen, V. Casella, S. F. Ngiow, O. Khan, Y. J. Huang, P. Yan, K. Nzingha, W. Xu, R. K. Amaravadi, X. Xu, G. C. Karakousis, T. C. Mitchell, L. M. Schuchter, A. C. Huang & E. J. Wherry (2020) Developmental Relationships of Four Exhausted CD8+ T Cell Subsets Reveals Underlying Transcriptional and Epigenetic Landscape Control Mechanisms. *Immunity,* 52**,** 825-841.e8.

Bocharov, G., J. Argilaguet & A. Meyerhans (2015) Understanding Experimental LCMV Infection of Mice: The Role of Mathematical Models. *Journal of Immunology Research,* 2015**,** 739706.

Bolouri, H., M. Young, J. Beilke, R. Johnson, B. Fox, L. Huang, C. C. Santini, C. M. Hill, A.-R. v. d. V. d. Vries, P. T. Shannon, A. Dervan, P. Sivakumar, M. Trotter, D. Bassett & A. Ratushny (2020) Integrative network modeling reveals mechanisms underlying T cell exhaustion. *Scientific Reports,* 10**,** 1-15.

Cao, X., Y. Liang, Z. Hu, H. Li, J. Yang, E. J. Hsu, J. Zhu, J. Zhou & Y.-X. Fu (2021) Next generation of tumor-activating type I IFN enhances anti-tumor immune responses to overcome therapy resistance. *Nature Communications,* 12**,** 1-11.

Chammas, P., I. Mocavini & L. Di Croce (2019) Engaging chromatin: PRC2 structure meets function. *British Journal of Cancer,* 122**,** 315-328.

Chang, J. T., V. R. Palanivel, I. Kinjyo, F. Schambach, A. M. Intlekofer, A. Banerjee, S. A. Longworth, K. E. Vinup, P. Mrass, J. Oliaro, N. Killeen, J. S. Orange, S. M. Russell, W. Weninger & S. L. Reiner (2007) Asymmetric T Lymphocyte Division in the Initiation of Adaptive Immune Responses. *Science,* 315**,** 1687-1691.

Chang, J. T., E. J. Wherry & A. W. Goldrath (2014) Molecular regulation of effector and memory T cell differentiation. *Nature Immunology,* 15**,** 1104-1115.

Chase, A. & N. C. P. Cross (2011) Aberrations of EZH2 in Cancer. *Clinical Cancer Research,* 17**,** 2613-2618.

Chen, J., I. F. López-Moyado, H. Seo, C.-W. J. Lio, L. J. Hempleman, T. Sekiya, A. Yoshimura, J. P. Scott-Browne & A. Rao (2019a) NR4A transcription factors limit CAR T cell function in solid tumours. *Nature,* 567**,** 530-534.

Chen, X., G. Cao, J. Wu, X. Wang, Z. Pan, J. Gao, Q. Tian, L. Xu, Z. Li & Y. Hao (2020) The histone methyltransferase EZH2 primes the early differentiation of follicular helper T cells during acute viral infection. *Cellular & molecular immunology,* 17**,** 247-260.

Chen, Y., R. A. Zander, X. Wu, D. M. Schauder, M. Y. Kasmani, J. Shen, S. Zheng, R. Burns, E. J. Taparowsky & W. Cui (2021) BATF regulates progenitor to cytolytic effector CD8+ T cell transition during chronic viral infection. *Nature Immunology,* 22**,** 996-1007.

Chen, Z., Z. Ji, S. F. Ngiow, S. Manne, Z. Cai, A. C. Huang, J. Johnson, R. P. Staupe, B. Bengsch, C. Xu, S. Yu, M. Kurachi, R. S. Herati, L. A. Vella, A. E. Baxter, J. E. Wu, O. Khan, J.-C. Beltra, J. R. Giles, E. Stelekati, L. M. McLane, C. W. Lau, X. Yang, S. L. Berger, G. Vahedi, H. Ji & E. J. Wherry (2019b) TCF-1-Centered Transcriptional Network Drives an Effector versus Exhausted CD8 T Cell-Fate Decision. *Immunity,* 51**,** 840-855.e5.

Consortium, T. E. P. (2012) An integrated encyclopedia of DNA elements in the human genome. *Nature,* 489**,** 57-74.

Cordero, F. J., Z. Huang, C. Grenier, X. He, G. Hu, R. E. McLendon, S. K. Murphy, R. Hashizume & O. J. Becher (2017) Histone H3.3K27M Represses p16 to Accelerate Gliomagenesis in a Murine Model of DIPG. *Molecular Cancer Research,* 15**,** 1243-1254.

Crawford, A., J. M. Angelosanto, K. L. Nadwodny, S. D. Blackburn & E. J. Wherry (2011) A role for the chemokine RANTES in regulating CD8 T cell responses during chronic viral infection. *PLoS pathogens,* 7**,** e1002098-e1002098.

Dobenecker, M.-W., J. S. Park, J. Marcello, M. T. McCabe, R. Gregory, S. D. Knight, I. Rioja, A. K. Bassil, R. K. Prinjha & A. Tarakhovsky (2018) Signaling function of PRC2 is essential for TCR-driven T cell responses. *Journal of Experimental Medicine,* 215**,** 1101-1113.

DR, S., K. J, B. RA, K. M, G. U, Y. KB, T. HW, G. J, L. MW, B. FD, T. P, C. RT, T. DC, A. TM, F. N, L. GM, W. EJ, Y. N & H. WN (2016) The epigenetic landscape of T cell exhaustion. *Science (New York, N.Y.),* 354.

DT, U., C. M, C. V, P. L, F. DP, C.-C. S, D. M, A. F, H. M, W. D, P. S, T. R, Z. D & H. W (2016) T Cell Factor 1-Expressing Memory-like CD8(+) T Cells Sustain the Immune Response to Chronic Viral Infections. *Immunity,* 45.

DuPage, M., G. Chopra, J. Quiros, W. L. Rosenthal, M. M. Morar, D. Holohan, R. Zhang, L. Turka, A. Marson & J. A. Bluestone (2015) The Chromatin-Modifying Enzyme Ezh2 Is Critical for the Maintenance of Regulatory T Cell Identity after Activation. *Immunity,* 42**,** 227-238.

EB, W., Y. DH, E. H, H. J, D. J, C. G, A. BJ, K. CL & B. DG (2013) Blockade of chronic type I interferon signaling to control persistent LCMV infection. *Science (New York, N.Y.),* 340.

Goswami, S., I. Apostolou, J. Zhang, J. Skepner, S. Anandhan, X. Zhang, L. Xiong, P. Trojer, A. Aparicio, S. K. Subudhi, J. P. Allison, H. Zhao & P. Sharma (2018) Modulation of EZH2 expression in T cells improves efficacy of anti–CTLA-4 therapy. *The Journal of Clinical Investigation,* 128**,** 3813-3818.

H, M., E. D, M. A, M. C, A. LP, M. T & T. PD (2021) PANTHER version 16: a revised family classification, tree-based classification tool, enhancer regions and extensive API. *Nucleic acids research,* 49.

Huang, J., J. Zhang, Z. Guo, C. Li, Z. Tan, J. Wang, J. Yang & L. Xue (2021a) Easy or Not—The Advances of EZH2 in Regulating T Cell Development, Differentiation, and Activation in Antitumor Immunity. *Frontiers in Immunology,* 12.

Huang, Z., S. G. Kang, Y. Li, J. Zak, N. Shaabani, K. Deng, J. Shepherd, R. Bhargava, J. R. Teijaro & C. Xiao (2021b) IFNAR1 signaling in NK cells promotes persistent virus infection. *Science Advances,* 7**,** eabb8087.

Hudson, W. H., J. Gensheimer, M. Hashimoto, A. Wieland, R. M. Valanparambil, P. Li, J.-X. Lin, B. T. Konieczny, S. J. Im, G. J. Freeman, W. J. Leonard, H. T. Kissick & R. Ahmed (2019) Proliferating Transitory T Cells with an Effector-like Transcriptional Signature Emerge from PD-1+ Stem-like CD8+ T Cells during Chronic Infection. *Immunity,* 51**,** 1043-1058.e4.

Im, S. J., M. Hashimoto, M. Y. Gerner, J. Lee, H. T. Kissick, M. C. Burger, Q. Shan, J. S. Hale, J. Lee, T. H. Nasti, A. H. Sharpe, G. J. Freeman, R. N. Germain, H. I. Nakaya, H.-H. Xue & R. Ahmed (2016) Defining CD8+ T cells that provide the proliferative burst after PD-1 therapy. *Nature,* 537**,** 417-421.

Jadhav, R. R., S. J. Im, B. Hu, M. Hashimoto, P. Li, J.-X. Lin, W. J. Leonard, W. J. Greenleaf, R. Ahmed & J. J. Goronzy (2019) Epigenetic signature of PD-1+ TCF1+ CD8 T cells that act as resource cells during chronic viral infection and respond to PD-1 blockade. *Proceedings of the National Academy of Sciences,* 116**,** 14113-14118.

Ji, Y., J. Fioravanti, W. Zhu, H. Wang, T. Wu, J. Hu, N. E. Lacey, S. Gautam, J. B. Le Gall, X. Yang, J. D. Hocker, T. M. Escobar, S. He, S. Dell'Orso, N. V. Hawk, V. Kapoor, W. G. Telford, L. Di Croce, S. A. Muljo, Y. Zhang, V. Sartorelli & L. Gattinoni (2019) miR-155 harnesses Phf19 to potentiate cancer immunotherapy through epigenetic reprogramming of CD8+ T cell fate. *Nature Communications,* 10**,** 1-12.

JT, C., C. ML, K. I, P. VR, M. CE, D. CS, M. EC, K. JS, S. NC, O. J, Y. CC, F. BI, O. HS, B. LJ, R. SM, K. GA, J. MS & R. SL (2011) Asymmetric proteasome segregation as a mechanism for unequal partitioning of the transcription factor T-bet during T lymphocyte division. *Immunity,* 34.

K, M., G. SS, L. Y, G. R, P. S, H. DC, P. M, Z. D, B.-S. F, F. MA, S. W & K. A (2017) Transcription Factor IRF4 Promotes CD8 + T Cell Exhaustion and Limits the Development of Memory-like T Cells during Chronic Infection. *Immunity,* 47.

Kakaradov, B., J. Arsenio, C. E. Widjaja, Z. He, S. Aigner, P. J. Metz, B. Yu, E. J. Wehrens, J. Lopez, S. H. Kim, E. I. Zuniga, A. W. Goldrath, J. T. Chang & G. W. Yeo (2017) Early transcriptional and epigenetic regulation of CD8+ T cell differentiation revealed by single-cell RNA sequencing. *Nature Immunology,* 18**,** 422-432.

Kang, N., M. Eccleston, P.-L. Clermont, M. Latarani, D. K. Male, Y. Wang & F. Crea (2020) EZH2 inhibition: a promising strategy to prevent cancer immune editing. *https://doi.org/10.2217/epi-2020-0186*.

KB, Y., T. P, M. GE, G. U, A. A. R, C. DE, W. SA, W. D, T. DC, C. RT, A. TM, K. AY, F. S, F. J, F. J, L. GM, H. WN & S. DR (2021) Epigenetic scars of CD8 + T cell exhaustion persist after cure of chronic infection in humans. *Nature immunology,* 22.

Khan, O., J. R. Giles, S. McDonald, S. Manne, S. F. Ngiow, K. P. Patel, M. T. Werner, A. C. Huang, K. A. Alexander, J. E. Wu, J. Attanasio, P. Yan, S. M. George, B. Bengsch, R. P. Staupe, G. Donahue, W. Xu, R. K. Amaravadi, X. Xu, G. C. Karakousis, T. C. Mitchell, L. M. Schuchter, J. Kaye, S. L. Berger & E. J. Wherry (2019) TOX transcriptionally and epigenetically programs CD8+ T cell exhaustion. *Nature,* 571**,** 211-218.

Kopitar-Jerala, N. (2017) The Role of Interferons in Inflammation and Inflammasome Activation. *Frontiers in Immunology,* 8.

Kurachi, M., R. A. Barnitz, N. Yosef, P. M. Odorizzi, M. A. DiIorio, M. E. Lemieux, K. Yates, J. Godec, M. G. Klatt & A. Regev (2014) The transcription factor BATF operates as an essential differentiation checkpoint in early effector CD8+ T cells. *Nature immunology,* 15**,** 373-383.

La Manno, G., R. Soldatov, A. Zeisel, E. Braun, H. Hochgerner, V. Petukhov, K. Lidschreiber, M. E. Kastriti, P. Lönnerberg, A. Furlan, J. Fan, L. E. Borm, Z. Liu,

D. van Bruggen, J. Guo, X. He, R. Barker, E. Sundström, G. Castelo-Branco, P. Cramer, I. Adameyko, S. Linnarsson & P. V. Kharchenko (2018) RNA velocity of single cells. *Nature,* 560**,** 494-498.

Langmead, B. & S. L. Salzberg (2012) Fast gapped-read alignment with Bowtie 2. *Nature Methods,* 9**,** 357-359.

Laugesen, A., J. W. Højfeldt & K. Helin (2016) Role of the polycomb repressive complex 2 (PRC2) in transcriptional regulation and cancer. *Cold Spring Harbor perspectives in medicine,* 6**,** a026575.

Lee, A. J. & A. A. Ashkar (2018) The Dual Nature of Type I and Type II Interferons. *Frontiers in Immunology,* 9.

M, B., B. I, B. NS, P. K, Y. A, G. F, B. N, H. A, S. I, B. Y & O. A (2019) Modulation of asymmetric cell division as a mechanism to boost CD8 + T cell memory. *Science immunology,* 4.

M, P., F. L, S. L, H. EL, C. S, S. M, S. AC, V. A, L. P, M. T, H. MD, W. JD, L. CS & S. A (2017) Chromatin states define tumour-specific T cell dysfunction and reprogramming. *Nature,* 545.

Marchetti, M., M.-N. Monier, A. Fradagrada, K. Mitchell, F. Baychelier, P. Eid, L. Johannes, C. Lamaze & S. Schmid (2006) Stat-mediated Signaling Induced by Type I and Type II Interferons (IFNs) Is Differentially Controlled through Lipid Microdomain Association and Clathrin-dependent Endocytosis of IFN Receptors. *https://doi.org/10.1091/mbc.e06-01-0076*.

Margueron, R. & D. Reinberg (2011) The Polycomb complex PRC2 and its mark in life. *Nature,* 469**,** 343-349.

Martinez, G. J., R. M. Pereira, T. Äijö, E. Y. Kim, F. Marangoni, M. E. Pipkin, S. Togher, V. Heissmeyer, Y. C. Zhang, S. Crotty, E. D. Lamperti, K. M. Ansel, T. R. Mempel, H. Lähdesmäki, P. G. Hogan & A. Rao (2015) The Transcription Factor NFAT Promotes Exhaustion of Activated CD8 + T Cells. *Immunity,* 42**,** 265-278.

McLane, L. M., M. S. Abdel-Hakeem & E. J. Wherry (2019) CD8 T Cell Exhaustion During Chronic Viral Infection and Cancer. *Annual Review of Immunology,* 37**,** 457-495.

Mognol, G. P., R. Spreafico, V. Wong, J. P. Scott-Browne, S. Togher, A. Hoffmann, P. G. Hogan, A. Rao & S. Trifari (2017) Exhaustion-associated regulatory regions in CD8+ tumor-infiltrating T cells. *Proceedings of the National Academy of Sciences,* 114**,** E2776-E2785.

MS, A.-H. (2019) Viruses Teaching Immunology: Role of LCMV Model and Human Viral Infections in Immunological Discoveries. *Viruses,* 11.

Muroyama, Y. & E. J. Wherry (2021) Memory T-Cell Heterogeneity and Terminology. *Cold Spring Harb Perspect Biol,* 13.

NH, F., N. DC & L. AE (2016) Integrated genome browser: visual analytics platform for genomics. *Bioinformatics (Oxford, England),* 32.

Osokine, I., L. M. Snell, C. R. Cunningham, D. H. Yamada, E. B. Wilson, H. J. Elsaesser, J. C. de la Torre & D. Brooks (2014) Type I interferon suppresses de novo virus-specific CD4
Th1 immunity during an established persistent
viral infection. ***Proceedings of the National Academy of Sciences of the United States of America****,* 111**,** 7409-7414.

Paley, M. A., D. C. Kroy, P. M. Odorizzi, J. B. Johnnidis, D. V. Dolfi, B. E. Barnett, E. K. Bikoff, E. J. Robertson, G. M. Lauer, S. L. Reiner & E. J. Wherry (2012) Progenitor and Terminal Subsets of CD8+ T Cells Cooperate to Contain Chronic Viral Infection. *Science,* 338**,** 1220-1225.

Pauken, K. E., M. A. Sammons, P. M. Odorizzi, S. Manne, J. Godec, O. Khan, A. M. Drake, Z. Chen, D. R. Sen, M. Kurachi, R. A. Barnitz, C. Bartman, B. Bengsch, A. C. Huang, J. M. Schenkel, G. Vahedi, W. N. Haining, S. L. Berger & E. J. Wherry (2016) Epigenetic stability of exhausted T cells limits durability of reinvigoration by PD-1 blockade. *Science (New York, N.Y.),* 354**,** 1160-1165.

Pauken, K. E. & E. J. Wherry (2015) Overcoming T cell exhaustion in infection and cancer. *Trends in Immunology,* 36**,** 265-276.

Platanias, L. C. (2022) Mechanisms of type-I- and type-II-interferon-mediated signalling. *Nature Reviews Immunology,* 5**,** 375-386.

Quigley, M., F. Pereyra, B. Nilsson, F. Porichis, C. Fonseca, Q. Eichbaum, B. Julg, J. L. Jesneck, K. Brosnahan & S. Imam (2010) Transcriptional analysis of HIV-specific

CD8+ T cells shows that PD-1 inhibits T cell function by upregulating BATF. *Nature medicine,* 16**,** 1147-1151.

Scott, A. C., F. Dündar, P. Zumbo, S. S. Chandran, C. A. Klebanoff, M. Shakiba, P. Trivedi, L. Menocal, H. Appleby, S. Camara, D. Zamarin, T. Walther, A. Snyder, M. R. Femia, E. A. Comen, H. Y. Wen, M. D. Hellmann, N. Anandasabapathy, Y. Liu, N. K. Altorki, P. Lauer, O. Levy, M. S. Glickman, J. Kaye, D. Betel, M. Philip & A. Schietinger (2019) TOX is a critical regulator of tumour-specific T cell differentiation. *Nature,* 571**,** 270-274.

Seo, H., J. Chen, E. González-Avalos, D. Samaniego-Castruita, A. Das, Y. H. Wang, I. F. López-Moyado, R. O. Georges, W. Zhang, A. Onodera, C.-J. Wu, L.-F. Lu, P. G. Hogan, A. Bhandoola & A. Rao (2019) TOX and TOX2 transcription factors cooperate with NR4A transcription factors to impose CD8. *Proceedings of the National Academy of Sciences,* 116**,** 12410-12415.

Seo, H., E. González-Avalos, W. Zhang, P. Ramchandani, C. Yang, C.-W. J. Lio, A. Rao & P. G. Hogan (2021) BATF and IRF4 cooperate to counter exhaustion in tumor-infiltrating CAR T cells. *Nature Immunology,* 22**,** 983-995.

SM, G., A. RA, G. T, K. SH & K. SM (2017) Polycomb Repressive Complex 2-Mediated Chromatin Repression Guides Effector CD8 + T Cell Terminal Differentiation and Loss of Multipotency. *Immunity,* 46.

Snell, L. M., T. L. McGaha & D. G. Brooks (2017) Type I Interferon in Chronic Virus Infection and Cancer. *Trends in Immunology,* 38**,** 542-557.

Sun, L., J. Wu, F. Du, X. Chen & Z. J. Chen (2013) Cyclic GMP-AMP Synthase Is a Cytosolic DNA Sensor That Activates the Type I Interferon Pathway.

T, S., S. A, M. S, L. CA & S. R (2021) Single-cell chromatin state analysis with Signac. *Nature methods,* 18.

TT, G. & Z. EI (2021) Type I Interferon Induction and Exhaustion during Viral Infection: Plasmacytoid Dendritic Cells and Emerging COVID-19 Findings. *Viruses,* 13.

Tumes, Damon J., A. Onodera, A. Suzuki, K. Shinoda, Y. Endo, C. Iwamura, H. Hosokawa, H. Koseki, K. Tokoyoda, Y. Suzuki, S. Motohashi & T. Nakayama (2013) The Polycomb Protein Ezh2 Regulates Differentiation and Plasticity of CD4+ T Helper Type 1 and Type 2 Cells. *Immunity,* 39**,** 819-832.

V, B., L. M, P. S, W. FA & T. FJ (2020) Generalizing RNA velocity to transient cell states through dynamical modeling. *Nature biotechnology,* 38.

Wang, C., M. Oshima, D. Sato, H. Matsui, S. Kubota, K. Aoyama, Y. Nakajima-Takagi, S. Koide, J. Matsubayashi, M. Mochizuki-Kashio, T. Nakano-Yokomizo, J. Bai, T. Nagao, A. Kanai, A. Iwama & G. Sashida (2018) Ezh2 loss propagates hypermethylation at T cell differentiation–regulating genes to promote leukemic transformation. *The Journal of Clinical Investigation,* 128**,** 3872-3886.

Wang, Y., J. Hu, Y. Li, M. Xiao, H. Wang, Q. Tian, Z. Li, J. Tang, L. Hu, Y. Tan, X. Zhou, R. He, Y. Wu, L. Ye, Z. Yin, Q. Huang & L. Xu (2019) The Transcription Factor TCF1 Preserves the Effector Function of Exhausted CD8 T Cells During Chronic Viral Infection. *Frontiers in Immunology,* 10**,** 169.

Weber, E. W., K. R. Parker, E. Sotillo, R. C. Lynn, H. Anbunathan, J. Lattin, Z. Good, J. A. Belk, B. Daniel, D. Klysz, M. Malipatlolla, P. Xu, M. Bashti, S. Heitzeneder, L. Labanieh, P. Vandris, R. G. Majzner, Y. Qi, K. Sandor, L.-C. Chen, S. Prabhu, A. J. Gentles, T. J. Wandless, A. T. Satpathy, H. Y. Chang & C. L. Mackall (2021) Transient rest restores functionality in exhausted CAR-T cells through epigenetic remodeling. *Science,* 372**,** eaba1786.

Wherry, E. J. (2011) T cell exhaustion. *Nature Immunology,* 12**,** 492-499.

Wherry, E. J., S.-J. Ha, S. M. Kaech, W. N. Haining, S. Sarkar, V. Kalia, S. Subramaniam, J. N. Blattman, D. L. Barber & R. Ahmed (2007) Molecular Signature of CD8+ T Cell Exhaustion during Chronic Viral Infection. *Immunity,* 27**,** 670-684.

Wherry, E. J. & M. Kurachi (2015) Molecular and cellular insights into T cell exhaustion. *Nature Reviews Immunology,* 15**,** 486-499.

Wolf, F. A., P. Angerer & F. J. Theis (2018) SCANPY: large-scale single-cell gene expression data analysis. *Genome Biology,* 19**,** 1-5.

Yang, X.-P., K. Jiang, K. Hirahara, G. Vahedi, B. Afzali, G. Sciume, M. Bonelli, H.-W. Sun, D. Jankovic & Y. Kanno (2015) EZH2 is crucial for both differentiation of regulatory T cells and T effector cell expansion. *Scientific reports,* 5**,** 1-14.

Yao, C., H.-W. Sun, N. E. Lacey, Y. Ji, E. A. Moseman, H.-Y. Shih, E. F. Heuston, M. Kirby, S. Anderson, J. Cheng, O. Khan, R. Handon, J. Reilley, J. Fioravanti, J.

Hu, S. Gossa, E. J. Wherry, L. Gattinoni, D. B. McGavern, J. J. O'Shea, P. L. Schwartzberg & T. Wu (2019) Single-cell RNA-seq reveals TOX as a key regulator of CD8+ T cell persistence in chronic infection. *Nature Immunology,* 20**,** 890-901.

Yi, J. S., M. A. Cox & A. J. Zajac (2010) T-cell exhaustion: characteristics, causes and conversion: T-cell exhaustion. *Immunology,* 129**,** 474-481.

Yigit, B., N. Wang, E. ten Hacken, S.-S. Chen, A. K. Bhan, A. Suarez-Fueyo, E. Katsuyama, G. C. Tsokos, N. Chiorazzi, C. J. Wu, J. A. Burger, R. W. Herzog, P. Engel & C. Terhorst (2019) SLAMF6 as a Regulator of Exhausted CD8+ T Cells in Cancer. *Cancer Immunology Research,* 7**,** 1485-1496.

Yoo, K. H. & L. Hennighausen (2012) EZH2 Methyltransferase and H3K27 Methylation in Breast Cancer. *International Journal of Biological Sciences,* 8**,** 59-65.

Zhang, Y., T. Liu, C. A. Meyer, J. Eeckhoute, D. S. Johnson, B. E. Bernstein, C. Nusbaum, R. M. Myers, M. Brown, W. Li & X. S. Liu (2008) Model-based Analysis of ChIP-Seq (MACS). *Genome Biology,* 9**,** 1-9.

Zheng, M. & L. Song (2020) Novel antibody epitopes dominate the antigenicity of spike glycoprotein in SARS-CoV-2 compared to SARS-CoV. *Cellular & Molecular Immunology,* 17**,** 536-538.

Zhou, Y., B. Zhou, L. Pache, M. Chang, A. H. Khodabakhshi, O. Tanaseichuk, C. Benner & S. K. Chanda (2019) Metascape provides a biologist-oriented resource for the analysis of systems-level datasets. *Nature Communications,* 10**,** 1-10.

Zhu, L., X. Zhou, M. Gu, J. Kim, Y. Li, C.-J. Ko, X. Xie, T. Gao, X. Cheng & S.-C. Sun (2022) Dapl1 controls NFATc2 activation to regulate CD8+ T cell exhaustion and responses in chronic infection and cancer. *Nature Cell Biology,* 24**,** 1165-1176.